ORNL/TM-2023/2951

ORNL Analysis of Leach-Burn-Leach Round-Robin Test Samples

John D. Hunn
Tyler J. Gerczak
Fred C. Montgomery
Grant W. Helmreich

June 2023

Approved for public release.
Distribution is unlimited.

OAK RIDGE National Laboratory

ORNL IS MANAGED BY UT-BATTELLE LLC FOR THE US DEPARTMENT OF ENERGY

ORNL/TM-2023/2951

Nuclear Energy and Fuel Cycle Division

ORNL ANALYSIS OF LEACH-BURN-LEACH ROUND-ROBIN TEST SAMPLES

John D. Hunn
Tyler J. Gerczak
Fred C. Montgomery
Grant W. Helmreich

Revision 0

June 2023

Work sponsored by
US DEPARTMENT OF ENERGY
Office of Nuclear Energy—Advanced Reactor Technologies
under the
Advanced Gas Reactor Fuel Development and Qualification Program

Prepared by
OAK RIDGE NATIONAL LABORATORY
Oak Ridge, TN 37831
managed by
UT-BATTELLE, LLC
for the
US DEPARTMENT OF ENERGY
under contract DE-AC05-00OR22725

CONTENTS

LIST OF FIGURES

LIST OF TABLES

ABBREVIATIONS

AGR	Advanced Gas Reactor Fuel Qualification and Development (Program)
CPFD	Coated Particle Fuel Development (Laboratory)
DRF	data report form
DUO_2	depleted uranium dioxide (kernels)
FB-CVD	fluidized-bed chemical vapor deposition
GIF	Generation IV International Forum
FIB	focused-ion-beam
HTGR	high-temperature gas-cooled reactor
ICP-MS	inductively coupled plasma mass spectrometry
INET	Institute of Nuclear and New Energy Technology
IPyC	inner pyrolytic carbon (TRISO layer)
KAERI	Korean Atomic Energy Research Institute
LBL	leach-burn-leach
max.	maximum
MDL	minimum detection limit
min.	minimum
NA	not applicable
NIST	National Institute of Standards and Technology
OPyC	outer pyrolytic carbon (TRISO layer)
ORNL	Oak Ridge National Laboratory
PIE	post-irradiation examination
ppm	parts per million
QC	quality control
SD	standard deviation
SiC	silicon carbide (TRISO layer)
SRM	Standard Reference Material
TRISO	tristructural-isotropic (coated particles)
UCO	mixture of uranium carbide and uranium oxide (kernels)
UO_2	uranium dioxide (kernels)
XCT	x-ray computed tomography
ZrO_2	zirconium dioxide (surrogate kernels)

ACKNOWLEDGMENTS

This work was sponsored by the US Department of Energy, Office of Nuclear Energy, Advanced Reactor Technologies as part of the Advanced Gas Reactor Fuel Development and Qualification Program. Analysis of leach solutions was provided by Tamara J. Keever, Ralph H. Ilgner, Kayron T. Rogers, and Marc R. Chattin of the Radioactive Materials Analytical Laboratory at Oak Ridge National Laboratory.

ABSTRACT

An international round-robin test to examine the consistency in leach-burn-leach (LBL) analysis of tristructural-isotropic- (TRISO-) coated particle fuel was conducted by three research organizations from the Generation IV International Forum member countries of the People's Republic of China, the Republic of Korea, and the United States of America. Two sets of round-robin test samples were exchanged for analysis. One set of samples consisted of a series of nonuranium-bearing, TRISO-coated zirconium dioxide particles seeded with up to four depleted uranium-bearing, TRISO-coated uranium dioxide (UO_2) particles, which had intentionally damaged coating layers to simulate either particles with either exposed-kernel defects (i.e., particles with a cracked TRISO coating that should be detected during preburn leaching) or particles with silicon carbide (SiC) defects (i.e., particles with an intact pyrocarbon coating and a hole in the SiC layer that should be detected during postburn leaching). These simulated samples also contained added powder with known quantities of impurities from a coal standard. The other sample set consisted of representative sublots of UO_2-TRISO particles fabricated in a production-scale coater, except they all contained depleted uranium instead of enriched uranium. In this report, the methodology used at Oak Ridge National Laboratory to conduct LBL analysis of the round-robin samples is presented, and the general results are summarized.

1. BACKGROUND

1.1 INTRODUCTION

The development and qualification of tristructural-isotropic- (TRISO-) coated particle fuel is ongoing in multiple member states associated with the Generation IV International Forum (GIF). A critical component of fuel qualification is the determination of particle defect fractions and impurities in as-fabricated fuel. These properties are typically determined through leach-burn-leach (LBL) analysis. A cooperative round-robin test focusing on LBL practices was undertaken by the GIF Very High Temperature Reactor System Fuel and Fuel Cycle Project Management Board. The participants in this LBL round-robin test were the People's Republic of China, the Republic of Korea, and the United States of America. The participating research organizations from each member state include the Chinese Institute of Nuclear and New Energy Technology (INET), the Korean Atomic Energy Research Institute (KAERI), and Oak Ridge National Laboratory (ORNL). The motivation of the GIF LBL benchmarking round-robin test was to explore consistency in LBL analysis results among the participating members and potentially understand the influence of LBL process variations on the accurate determination of the measured fuel properties.

The TRISO-coated particle fuel design relevant to high-temperature gas-cooled reactors (HTGRs), such as the graphite-moderated prismatic-core or pebble-bed HTGRs, consists of an encapsulated fissile fuel kernel that is typically uranium dioxide (UO_2), or a mixture of uranium carbide and uranium oxide called "UCO". The kernel is coated with a porous carbon buffer layer and three isotropic layers consisting of inner pyrolytic carbon (IPyC), chemical vapor deposition silicon carbide (SiC), and outer pyrolytic carbon (OPyC). The individual TRISO particles are then typically overcoated with a resinated-graphite powder and pressed into either a spherical pebble or cylindrical compact, depending on reactor design. The pressed fuel forms are then heated to carbonize the resin, leaving a graphitic matrix that encases the particles in the final fuel form (Petti et al. 2010).

Certain impurities and coating defects in as-fabricated TRISO fuel can affect the reactor source term and potentially limit the lifetime of the fuel. Impurities in the OPyC or matrix can have deleterious effects on in-reactor performance if the impurities react with the TRISO layers, especially metallic impurities that react with SiC at elevated temperature. If it undergoes fission, uranium not contained within a normally functioning SiC layer may contribute to radionuclide release into the HTGR structural graphite and/or coolant during operation. This uncontained uranium may be in the kernels of particles with coating defects or may be present as uranium contamination in the OPyC layer or graphitic matrix.[1] Uranium contamination may come from uranium in the graphite used to make the matrix or may be introduced during fuel processing. Two as-fabricated defects measured via LBL to evaluate TRISO fuel quality are exposed-kernel defects (kernels not retained within gas-tight/liquid-tight layers) and SiC defects (kernels not encapsulated by a normally retentive SiC layer but with at least one gas-tight/liquid-tight pyrolytic carbon layer).[2] Exposed-kernel defects might be caused by adverse handling that can result in cracks propagating through all coating layers of a TRISO particle. Anomalies that may occur during SiC coating, such as soot inclusions, may result in SiC defects.

Leach-burn-leach analysis is also used during post-irradiation examination (PIE) to gain insight into TRISO fuel performance by measuring the amount of uranium and radionuclides not contained within retentive SiC layers. Analogues to exposed-kernel defects and SiC defects in as-fabricated particles may be detected in irradiated TRISO fuels before or after safety testing. Complete TRISO layer failure resulting in exposed-kernel defects can occur via unexpected chemical or mechanical processes, such as

[1] "Uranium contamination" typically refers to uranium not associated with coating defects and is used in that way herein.
[2] By convention, particles are only classified as having "SiC defects" if they are not counted as having "exposed-kernel defects", as the latter is a more serious defect and often has a lower acceptance limit on the allowable defect fraction.

reaction with metallic inclusions or layer fracture due to internal pressurization. Occurrences of SiC failure in the absence of complete TRISO failure have been observed due to localized palladium attack of the SiC layer in UCO kernel fuel or carbon monoxide gas corrosion of the SiC layer in UO_2 kernel fuel, in which the SiC attack in both cases is often more intense at regions exposed by degraded IPyC/SiC interfaces (Hunn et al. 2016; Morris et al. 2018). Select radionuclides have also been observed to be present outside of intact TRISO particles in the OPyC and graphitic matrix material (Demkowicz et al. 2015). The release of radionuclides in the absence of defective or failed TRISO coatings (i.e., via migration out of the kernels and diffusion through normal SiC layers) can contribute to the reactor source term, particularly for reactor designs that subject the SiC to very high temperatures.

1.2 GENERAL LEACH-BURN-LEACH ANALYSIS AT ORNL

Detailed discussion of the ORNL LBL process can be found in the references by Hunn and Baldwin (Hunn 2013, Hunn et al. 2013, Baldwin et al. 2014). The LBL analysis is performed by following a set of established procedures developed as part of the US Department of Energy Advanced Gas Reactor Fuel Qualification and Development (AGR) Program, which is focusing on UCO TRISO-coated particle fuel in prismatic compacts (Petti et al. 2010). Separate procedures have been developed for the LBL analysis of as-fabricated fuel compacts and for PIE of irradiated fuel compacts. Although the processes are similar, variation is present in the handling and apparatuses used to perform the analysis. The description of the LBL approach in this report focuses on the process developed for as-fabricated fuel defects and impurity analysis. Specific discussion of the methodology is provided in Section 2.

The general LBL approach at ORNL includes three to four phases, depending on whether particles are loose or have been overcoated with a resinated graphite powder and compacted into a consolidated fuel form. The first phase is a deconsolidation if the fuel is in a compacted form. Following deconsolidation, the matrix debris and TRISO particles are subjected to a preburn leaching, a burn to remove exposed carbon, and postburn leaching. In the deconsolidation phase, the compacted form is electrolytically deconsolidated in a nitric acid electrolyte to break up the matrix material and access the particles. The graphitic matrix is selectively disassociated due to intercalation of nitrate anions and nitric acid between the basal planes of the graphite. This results in disintegration of the graphite structure and liberation of the particles. Following deconsolidation, particles and matrix debris are subjected to a preburn leach. Deconsolidation and preburn leaching generally identifies uranium contamination and other impurities in the matrix and on the surface of the OPyC layer. Exposed-kernel defects, such as cracked particles, are also identified in the deconsolidation and preburn leach phases as the uranium in the kernel is accessible to the nitric acid. Following the preburn leach phase, the remaining material is heated in air to oxidize exposed carbon and unleached metals. This burn phase includes removal of the carbonaceous matrix debris, the OPyC, and any internal IPyC and buffer layers that are exposed to air through a defective SiC layer. Some uranium contamination or metallic impurities may not be dissolved in the preburn leach phase, and they become more accessible and/or more soluble in nitric acid after the burn phase (Hunn et al. 2013). Metallic elements, including those in the kernel, may also be oxidized if they are exposed during the burn by removal of the IPyC and buffer in particles with defective SiC. Postburn leaching follows the burn phase. During postburn leaching, kernels in particles with defective SiC are leached, and the amount of dissolved uranium can be used to enumerate how many are present. Oxidized metallic impurities that are solubilized in the postburn leach phase are also measured. The implementation of the LBL process allows for impurities, uranium contamination, exposed-kernel defects, and SiC defects in as-fabricated TRISO fuel to be identified, quantified, and further examined, providing greater insight into the overall fuel quality and the cause of detected fuel failure.

1.3 SAMPLES FOR LEACH-BURN-LEACH ROUND-ROBIN TEST

The cooperative round-robin test included two types of samples for comparative LBL analysis. The two types were (1) representative sublots containing uranium-bearing TRISO particles produced in a

production-size coater and (2) simulated samples containing ~10,000 surrogate (nonuranium-bearing) TRISO particles to which were added up to four uranium-bearing TRISO particles with simulated defects in addition to carbon powder containing a known amount of various relevant impurities (Gerczak et al. 2022). The series of simulated samples provided to each participant included examples of both types of defective particles relevant to LBL (exposed-kernel defects and SiC defects). Because the simulated samples had known numbers and types of defective particles and known masses of various impurities, they were useful in exploring the accuracy and consistency of the LBL methods employed by each participant. The analysis of the representative sublots provided a way to compare results obtained from analysis of multiple samples from the same coating batch that were representative of typical TRISO fuel.

The representative sublots consisted of TRISO particles with depleted-uranium UO_2 (DUO_2) kernels and were supplied by INET. Participants were provided four samples riffled from a single large parent lot so that measured results could be statistically compared. Three ~40 g representative-TRISO samples were to be subjected to LBL analysis by each participant to measure defect fractions. One ~10 g sample was reserved for determining the average uranium loading per particle.

The simulated samples were supplied to each participant by ORNL. Details on the production of the particles with simulated defects can be found in ORNL/TM-2015/722, *Preparation of Simulated LBL Defects for Round-Robin Experiment* (Gerczak et al. 2022). Particles with simulated defects were produced using DUO_2 TRISO particles fabricated at ORNL in coating batch DUN500S-10A. The exposed-kernel defects were produced by subjecting fully TRISO-coated particles to a single-point impact. This resulted in fractures propagating through all the TRISO layers and exposing the kernel. These simulated defects represent one type of exposed-kernel defect that should be identified during the preburn leach phase of the LBL analysis. Each particle with a simulated exposed-kernel defect was verified with x-ray computed tomography (XCT) before adding to the simulated samples used for the round-robin test. The XCT-generated cross section (tomogram) in Figure 1-1 shows a fracture that exposed the kernel in a particle with a simulated exposed-kernel defect. Particles with SiC defects were simulated using burned-back DUO_2 TRISO particles from batch DUN500S-10A. The burnback was implemented to remove the OPyC layer because of limitations in the dimensions of the hole that could be produced with the method used to fabricate the simulated defects (Gerczak et al. 2022). A dual-beam focused-ion-beam (FIB), scanning-electron microscope was used to locally mill a 25 μm diameter hole through the SiC layer, exposing the IPyC layer. Figure 1-2 shows an example of a simulated SiC defect produced in a particle for the LBL round-robin test. Each particle with a simulated SiC defect was verified with x-ray radiography before adding to the simulated samples used for the round-robin test.

A series of seven individual simulated samples were supplied to each participant. Each contained ~10,000 surrogate coated particles with ~500 μm diameter zirconium dioxide (ZrO_2) kernels and a known quantity of an impurity standard, namely National Institute of Standards and Technology (NIST) Standard Reference Material (SRM) 1632d, which contained relevant concentrations of many of the elements of interest to fuel performance and/or PIE analysis. One of the seven samples in each series contained no particles with simulated defects to serve as a baseline. Three samples contained either one, two, or four particles with simulated exposed-kernel defects. The remaining three samples contained either one, two, or four particles with simulated SiC defects. The samples were labeled with the acronym for the participating research institution and an alphabetical sequence (e.g., ORNL-A through ORNL-G). The number of simulated defects in each sample were not shared with the participants to maintain a blind study. Requested reporting included the amounts of uranium and relevant impurities measured in each leach phase, as well as the number and type of defect in each simulated sample. After each institution had completed and reported on LBL analysis of their simulated sample set at a GIF meeting, information on the population of particles with simulated defects and the masses of the added impurities was distributed to participants via a revision to ORNL/TM-2015/722 (Gerczak et al. 2022). Appendix A contains this information for simulated samples ORNL-A through ORNL-G.

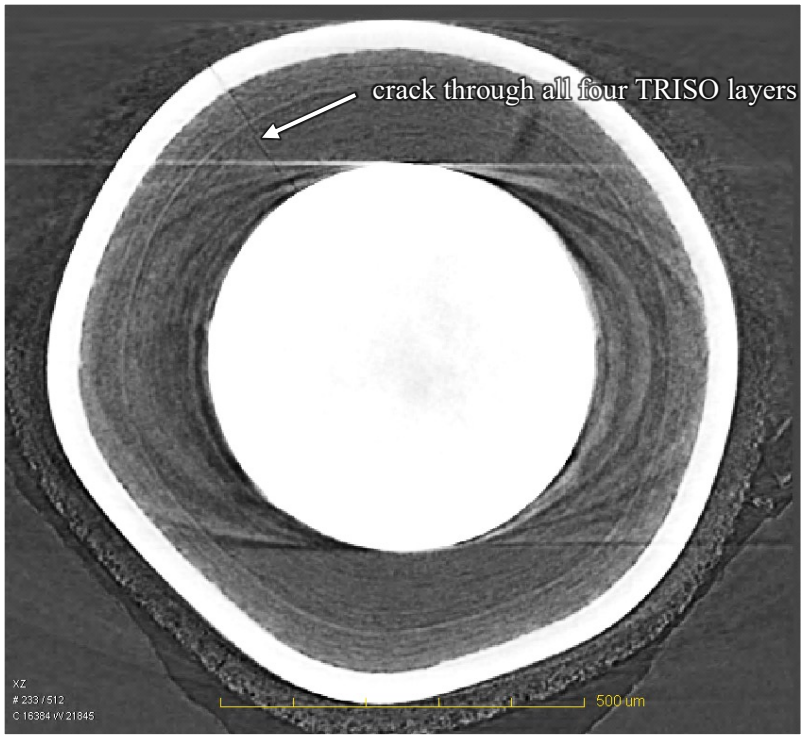

Figure 1-1. XCT tomogram of a DUN500S-10A particle with a simulated exposed-kernel defect that was produced by single-point impact. Image from Gerczak et al. (2022).

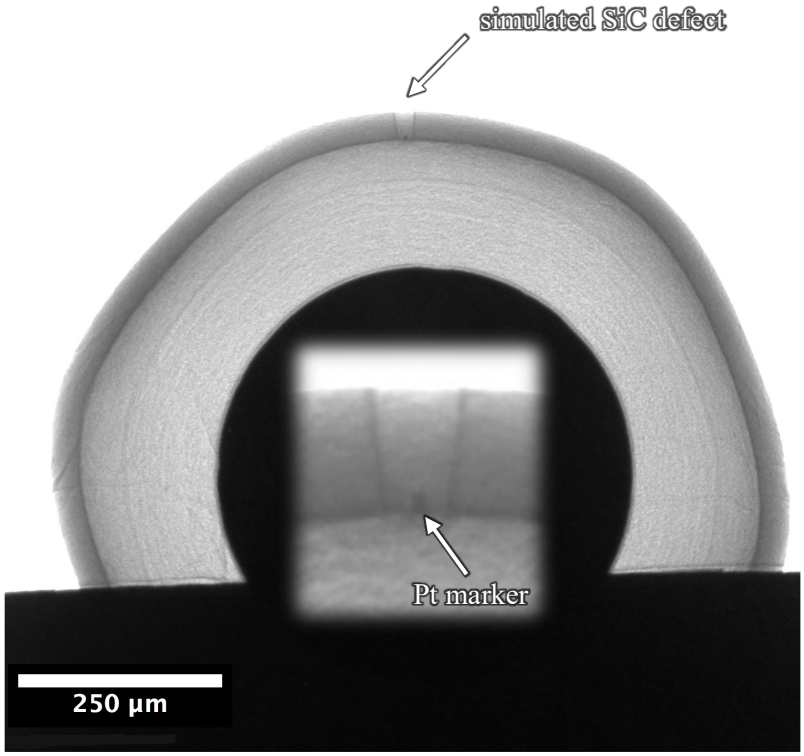

Figure 1-2. X-ray radiograph showing a simulated SiC defect that terminates near the IPyC/SiC interface. Inset shows a close-up of the simulated defect with a platinum marker to mark the bottom of the milled feature. Images from Gerczak et al. (2022).

2. SUMMARY OF METHODOLOGY FOR LEACH-BURN-LEACH ANALYSIS AT ORNL

2.1 LEACH-BURN-LEACH METHODOLOGY

To provide the necessary background and terminology needed to understand the results and subsequent discussion of the LBL analyses performed on round-robin test samples at ORNL, the methodology of compact deconsolidation and LBL will be described in this section. The data acquisition method described herein focuses on the analysis of as-fabricated fuel and does not address additional steps or equipment used when working in a hot cell with irradiated fuel during PIE, which have been described in ORNL/TM-2013/236 (Hunn et al. 2013). A general flowchart outlining the various phases of the LBL process is shown in Figure 2-1.

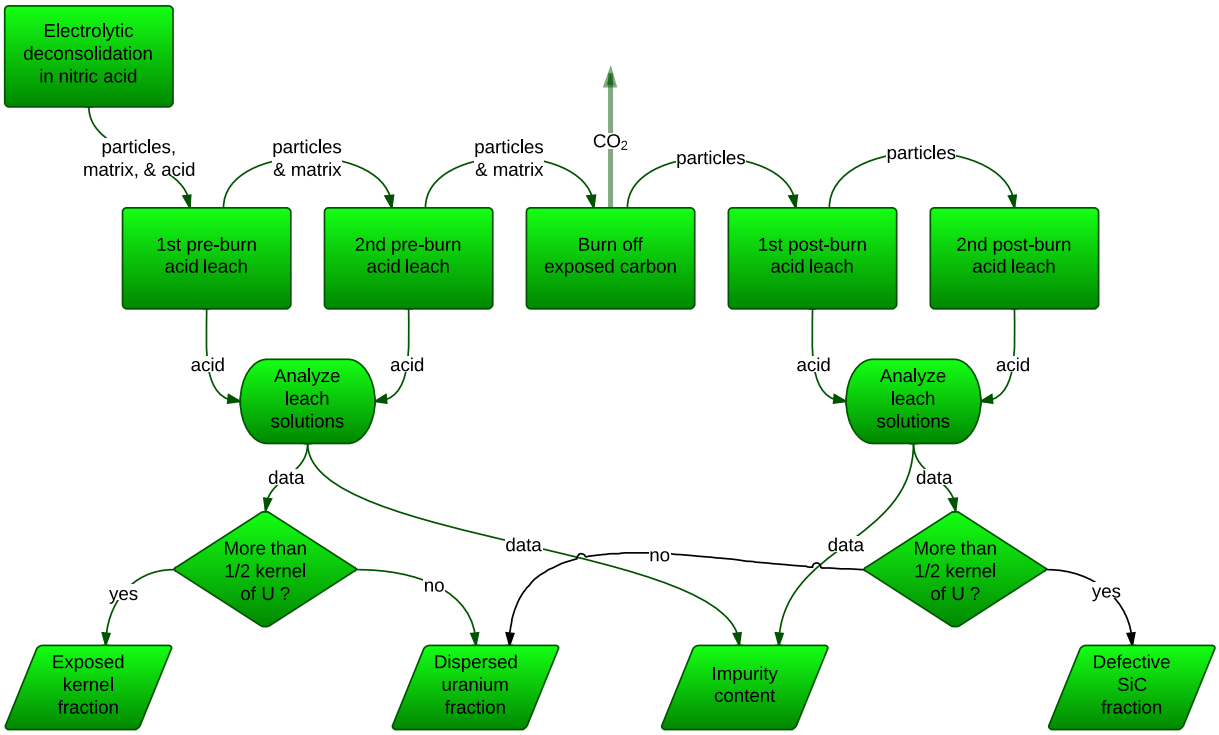

Figure 2-1. Flowchart of the LBL process demonstrating the individual phases in the analysis and determination of particle defect properties. Flowchart from Hunn (2013).

Before starting analysis, all glassware is cleaned, either by using standard analytical chemistry methods, such as ultrasonic cleaning and multiple water rinses, or by rinsing with high-purity, ~70% concentrated nitric acid. Both these cleaning processes are followed by a final rinse with high-purity water to minimize background levels for the impurities of interest. If any potential issues are noted with glassware to be used in the LBL process, the glassware is discarded and replaced. A blank is also typically run concurrently with all samples being subjected to the LBL process. The blank consists of just the high-purity acid used for leaching (no fuel sample) and is run to determine background levels. All steps associated with the standard LBL process are followed for the blank.

To perform the deconsolidation, a known volume of electrolyte (high-purity, ~70% concentrated nitric acid) is added to the quartz vessel used in the deconsolidation process (Figure 2-2b). Enough liquid is used to cover the residue from the compacts to be deconsolidated. The compact to be deconsolidated is placed in the bottom of the deconsolidation tube (Figure 2-2a), which is inserted into the quartz vessel in such a fashion that only the bottom (<5 mm) of the compact is submerged in the electrolyte. The anode

rod, which is a thick-walled capillary tube with a platinum wire threaded through the center, is positioned on top of the compact. A second platinum wire is placed in the electrolyte in the quartz vessel but not in contact with the compact. The submerged tip of the compact forms the anode and the platinum wire in the electrolyte forms the cathode of the electrolytic cell. The compact is deconsolidated at a power of 1–3 W. Deconsolidation above 10 W may damage the fuel and is avoided. During deconsolidation, the liberated particles and matrix debris are collected at the bottom of the quartz vessel. After the deconsolidation is complete, any remaining debris is rinsed from the deconsolidation tube into the quartz vessel containing the particles, matrix debris, and deconsolidation acid using additional high-purity, ~70% concentrated nitric acid.

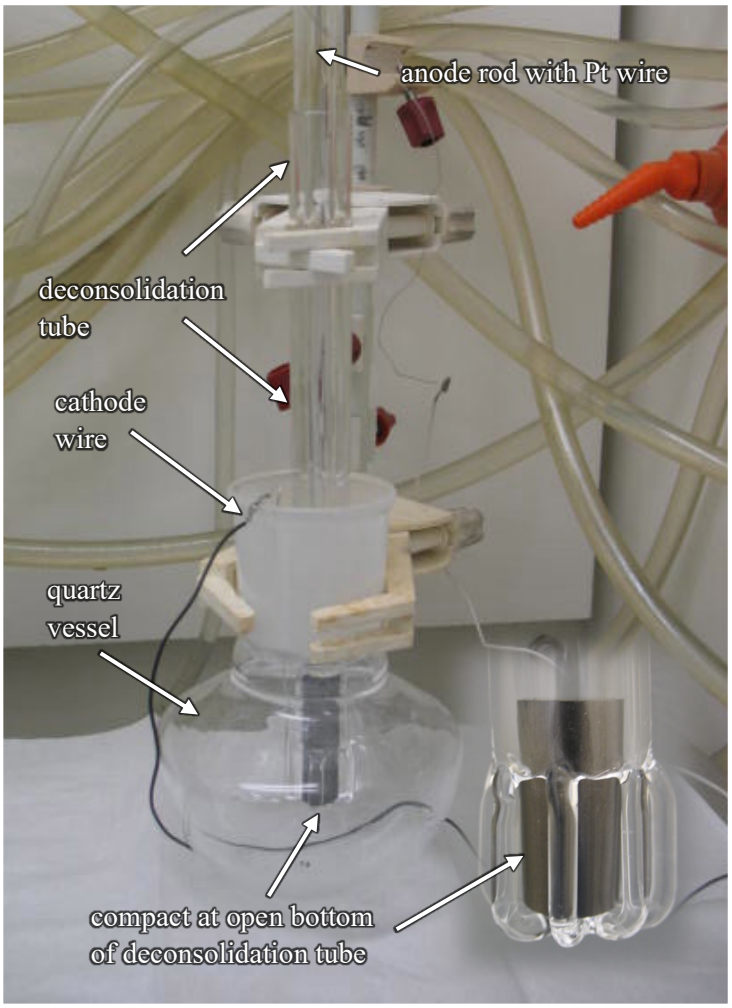

Figure 2-2. Electrolytic deconsolidation assembly showing compact deconsolidation rig.
Inset shows compact located at bottom of deconsolidation tube.

To begin the preburn leach process, additional high-purity, ~70% concentrated nitic acid is added to the quartz vessel containing particles, matrix debris, and acid, if needed to fully submerge the sample. The quartz vessel is then placed in a heating mantle and an LBL reflux apparatus (quartz vessel, adapter, condenser, and bump trap) is assembled (Figure 2-3). The heating mantle is then slowly ramped to just below the boiling point of the nitric acid (~120°C) and held at temperature for 24 h. Care must be taken to avoid overheating the quartz vessel, which can result in bumping of the liquid, as this may eject particles from the flask, possibly damaging them and causing atypical results.

Figure 2-3. Leaching station showing six LBL reflux apparatuses.

After hot leaching for 24 h, the system is cooled to room temperature and the acid is separated from the solids. As much of the acid as possible is decanted and/or pipetted from the vessel into 50 ml centrifuge tubes, while leaving as much of the solid material in the quartz vessel as possible. Capped spin-down tubes are agitated with a vortex mixer to suspend the matrix debris and then spun in a centrifuge at a radius of 16.1 cm for 15 min at 4250 revolutions per minute (a relative centrifugal field of ~3250), which results in the particles and matrix debris being separated from the acid. The acid is then decanted and/or pipetted from the spin-down tubes into a clean, certified Class A graduated cylinder large enough to hold this acid and liquid from two subsequent acid rinses. The two nitric acid rinses are performed to more thoroughly collect uranium and impurities dissolved during the hot leaching. Each acid rinse involves washing down the inner surfaces of the condenser and adapter by squirting with nitric acid, which is collected and swirled in the quartz vessel with the particles and matrix debris. The same steps associated with the separation and collection of the acid from the hot leach are performed with the acid rinse solutions, which are ultimately added to the liquid in the certified Class A graduated cylinder to make up the total collected leachate from first preburn leach. The volume of the leachate is recorded to allow for later determination of the masses of uranium and other impurities in the leachate by measuring the concentrations in a representative aliquot. The leachate is mixed to ensure uniform concentrations and then two aliquots are taken. One aliquot is analyzed by inductively coupled plasma mass spectrometry (ICP-MS) to determine the concentrations of uranium and selected impurities, while the other is retained as a backup.

At a minimum, a second preburn leach is performed (Figure 2-1) to leach the sample more thoroughly before the burn and provide information on whether a sufficient fraction of accessible uranium was dissolved after two 24 h hot leaches. The residue remaining in the centrifuge tubes from the previous leach is washed with high-purity, ~70% concentrated nitic acid back into the vessel containing the rest of the particles and matrix debris, and the process described above for the first preburn leach is repeated. Although often impractical due to schedule constraints, the best practice is to not proceed with the burn phase until the leachates from the first, second, and any optional additional preburn leaches are analyzed. This allows for additional preburn leaches to be performed if incomplete leaching of uranium from particles with exposed-kernel defects is observed. Incomplete leaching is indicated when a second or succeeding preburn leachate presents a uranium content that is above the minimum detection limit (MDL)

of the analysis technique and more than a significant fraction (typically determined to be 10–20%) of the cumulative amount of uranium observed in the preceding preburn leachate(s).

Before the burn phase, two water rinses are performed to remove residual nitric acid from the quartz vessel, particles, and matrix debris. Each water rinse entails washing down the inner surfaces of the adapter and condenser by squirting with water, which is collected and swirled in the quartz vessel with the particles and matrix debris. Using the same methodology applied to the separation and collection of the acid leachates, the water in the vessel after each rinse is decanted and/or pipetted into the centrifuge tubes used for the second preburn leach, followed by vortex mixing, centrifuging, and collection of the separated water. Ideally, the volume of the total collected water rinsate is determined and an aliquot is analyzed to measure any residual uranium or impurities picked up during the water rinses. This provides additional feedback about the adequacy of the processes for collecting the acid leachate, and significant values from the rinsate analysis can be added to the preburn leachate data. After removal of the water rinsate, the residual material in the spin-down tubes is transferred back to the quartz vessel by rinsing the tubes with high-purity water or methanol. Prior to the burn phase, the remaining liquid in the quartz vessel is evaporated by heating in a drying oven.

To complete the burn phase, the quartz vessel is placed in a specially designed burn apparatus like the one shown in Figure 2-4. The apparatus has an air inlet to provide additional oxygen to the vessel. Without airflow, the oxygen concentration in the vessel may be depleted enough to significantly slow the oxidation processes during the burn. The burn apparatus is placed in a muffle furnace, and an airflow of ~500 cm^3/min is established. The furnace temperature is then ramped to 750°C and held there for 72 h. After 72 h, the furnace is cooled, and the contents of the quartz vessel are visually examined to ensure that the burn phase was successful. As previously discussed in Section 1.2, the burn phase removes the matrix debris and exposed carbonaceous TRISO coating layers. After the OPyC burns off, oxygen eventually reaches the IPyC and buffer in particles with defective SiC, removing those layers as well. The kernel in a particle with defective SiC will also be oxidized, making it easier to dissolve during the postburn leach. Select impurities not leached from the matrix debris during the preburn leaching may also be oxidized, resulting in a more soluble form during the postburn leach.

Figure 2-4. Two station covered air supply apparatus to facilitate the burn phase.

The steps performed in the postburn leach phase do not differ from the preburn leach phase and use the same apparatus and setup. A minimum of two postburn leaches are performed. As for preburn leaching, to ensure leaching is complete, additional leaches are warranted until the uranium content in the last postburn leachate is below the MDL or less than a significant fraction (typically determined to be 10–20%) of the uranium previously measured during the postburn leaching phase. After postburn leaching, a water rinse is performed identical to that done between the preburn leach and burn phases. At the end of the postburn phase, what remains are the burned-back particles and any undissolved residual ash. This material can be dried and reserved for additional analysis, if desired.

As discussed in Section 1.1, LBL analysis of as-fabricated TRISO fuel is typically used to quantify noncarbon elements outside the confinement of the SiC coating layer, including uranium present as contamination and certain metallic impurities relevant to fuel performance and the production process. The metallic impurities of interest are generally iron, chromium, manganese, cobalt, nickel, calcium, aluminum, vanadium, and titanium. The masses of uranium and relevant impurities removed during each leach are calculated by multiplying the measured concentrations in the analyzed aliquot by the total volume of leachate measured in the certified Class A graduated cylinder. The leached masses are then converted to values independent of the size of the individual LBL samples, such as mass fractions or mass per individual fuel element, and these values are typically averaged over all analyzed samples for statistical comparison to the specified limits, with the assumption that the uranium contamination and impurity content are sufficiently dispersed to treat as variable properties (Kercher and Hunn 2005). Typically, uranium contamination can only be measured in samples with no exposed-kernel defects or SiC defects, because the uncertainty in uranium leached from one defective particle is usually higher than the uranium contamination level.

To determine the number of particles with exposed-kernel defects or SiC defects, the total mass of uranium in the preburn or postburn leachates, respectively, is divided by the average mass of uranium per particle (which is measured as described in Section 2.2) to calculate how many particle equivalents of uranium were in the leachates. Ideally, the values for preburn and postburn particle equivalents of uranium should be near integral values and representative of the number of exposed-kernel defects and SiC defects, respectively. Deviations from integral particle equivalent values are expected to result from measurement uncertainty and variation in the amount of uranium in each particle, both of which should be less than 20%. Uranium contamination can also contribute to deviations from integral particle equivalent values, and this contribution is dependent on both the level of uranium contamination and the size of each fuel sample analyzed by LBL. If necessary, corrections can be made by subtracting out the estimated contribution from uranium contamination. Deviations in the total preburn or postburn dissolved uranium from integral particle equivalent values that are greater than what is expected from measurement uncertainty, variation in particle inventory, and uranium contamination may indicate incomplete leaching and warrant additional examination. In practice, if the particle equivalents of uranium dissolved in the leachates before or after the burn is less than a specified value, then the dissolved uranium is assumed to be from uranium contamination rather than defective particles. The numbers of exposed-kernel defects and SiC defects in all sampled material from an evaluated fuel lot are typically compared to the specified limits with the assumption that these are attribute properties. Therefore, the particle equivalents of uranium leached from each sample before or after the burn are rounded to the nearest whole number and binomial statistics are used to calculate whether these values provide sufficient confidence that the defect fractions in the evaluated composite are below allowable limits (Kercher and Hunn 2005).

During fuel fabrication for the AGR program, the specified value for delineation between defective particles and uranium contamination was 0.5 particle equivalents (Marshall 2017). However, a cutoff value of 0.5 particle equivalents could result in misidentifying the uranium from one defective particle with a partially leached kernel as uranium contamination if other indicators are ignored, such as the relative amount of uranium in the leachates from sequential leaches. Therefore, a lower cutoff value might be considered as an improved metric, especially if it were informed by the average uranium

contamination measured from multiple fuel samples containing no defective particles and supplemental characterization of defective particles after LBL.

2.2 SUPPLEMENTAL ANALYSIS: AVERAGE URANIUM LOADING

The average mass of uranium per particle (average uranium loading) is required to determine the particle equivalents of uranium leached during LBL, as discussed in Section 2.1, and it is also used for nuclear material control and determination of the number of TRISO particles included in each compact or pebble to achieve the target fuel loading. The general process involves measuring the uranium content in a sample of particles and dividing by the number of particles in the sample. The number of particles in the sample is typically determined by weighing the sample and dividing by a previously determined average particle weight obtained by weighing and counting five to ten random samples of ~200 particles each. Three separate samples of several thousand particles are measured concurrently to determine the mean uranium loading. The mass of the particles is measured for each sample. Each sample is then transferred to a clean quartz vessel and burned in air at 900°C for at least 3 h to remove the OPyC layer from the particles. The burned-back particles are then transferred to a polyethylene bottle with ~3 g of 3 mm diameter zirconia milling media, and the particles are crushed in a Spex mill for ~10 min. These steps are performed to ensure that the uranium in the kernels is readily accessible during subsequent burning and leaching.

The polyethylene bottle containing the crushed particles is placed into a quartz reflux vessel and heated in a muffle furnace. The furnace is first brought to 350°C at a ramp rate of 15°C/min and held at temperature for 15 min. The furnace is then increased to 600°C at a rate of 1°C/min to burn off the polyethylene bottle, then to 750°C at a rate of 15°C/min, and the samples are held at 750°C for at least 5 h. These thermal exposure steps are performed to oxidize the carbon layers and convert the uranium compounds in the kernels to U_3O_8, which is readily soluble in nitric acid. After the quartz vessel is cool, high-purity, 70% concentrated nitric acid is added to submerge the sample, the vessel is placed in the heating mantle, and an LBL reflux apparatus is assembled (Figure 2-3), as described in Section 2.1. The acid solution containing crushed and oxidized particles is brought to a moderate boil for at least 4 h to dissolve the uranium. The contents of the vessel are then subjected to the same steps associated with separation and collection of the preburn leachate described in Section 2.1 and analysis and backup aliquots are taken. This includes decanting and/or pipetting the hot leach acid into spin-down tubes, centrifuging the samples, transferring the separated solutions to a certified Class A graduated cylinder, performing two acid rinses, and measuring the total volume of the collected leachate before collecting the two aliquots. Like the LBL preburn and postburn leaching processes, the leaching of the crushed and oxidized particles for uranium loading analysis is completed a minimum of two times. To confirm complete leaching of the uranium, the residual ash remaining in the vessel is transferred to filter paper via deionized water and allowed to dry. Another piece of filter paper is placed over the top of the sample and the activity is measured using a Geiger counter. The activity of ~0.1% of the total number of particles analyzed is measured in the same fashion. This equates to ~4 particles for a sample of ~3500–4500 particles. If the activity of the residual ash is less than the activity of the particles representing ~0.1% of each uranium loading sample, then the uranium is considered sufficiently leached and no additional leaching is required. Uranium concentrations in aliquots from the first leach are measured via Davies-Gray titration, while the lower concentrations in aliquots from the second leach are measured via ICP-MS. As for LBL, the measured uranium concentrations in the aliquots are converted to the total mass in each leachate by multiplying by the associated volume of collected leachate. The masses in the first and second leachates are summed, and this total mass is then divided by the number of particles to obtain the average uranium loading per particle. The number of particles is estimated by dividing the measure mass of particles in the sample by the average particle weight (see Section 3.1).

3. ANALYSIS OF REPRESENTATIVE SUBLOTS

Four samples containing TRISO-coated DUO_2 kernels were received from INET. These samples were representative of particles produced by a production-scale coater and were randomly riffled sublots from a single coating batch. The four representative sublots sent to ORNL were labeled as ORNL-DUO2-01T through ORNL-DUO2-04T and are shown in their shipping container in Figure 3-1. The representative sublots were inspected and weighed upon receipt. No unexpected matter was observed when the contents in the vials were transferred to the weigh pan. Table 3-1 lists the INET reported weights of each representative sublot, and the weights measured at ORNL upon receipt. The weight data for all samples showed good agreement between the measurements at both the shipping and receiving institutions, with the small differences likely a factor of weighing on balances with different accuracies. ORNL weights were obtained using a four decimal place analytical balance.

Figure 3-1. Photograph of as-received INET sample vials.

Table 3-1. Comparison of the sample weights reported by INET and ORNL

Sample	Weight (INET)	Weight (ORNL)
ORNL-DUO2-01T	41.81 g	41.8176 ± 0.0002 g
ORNL-DUO2-02T	41.30 g	41.3057 ± 0.0002 g
ORNL-DUO2-03T	38.92 g	38.9239 ± 0.0002 g
ORNL-DUO2-04T	10.00 g	9.9986 ± 0.0002 g
Total Weight	132.03 g	132.0458 ± 0.0004 g

Note: Differences in measured weights are within the presumed ±0.01 g uncertainty in the INET reported weights.

The planned analysis of the representative sublots included both LBL and uranium loading. The LBL analysis was performed on the three larger sublots (ORNL-DUO2-01T through ORNL-DUO2-03T) in the as-received condition. The 10 g representative sublot designated for uranium loading, ORNL-DUO2-04T, was rotary riffled to produce three equivalent uranium loading subsamples (ORNL-DUO2-04T-A01, ORNL-DUO2-04T-B01, and ORNL-DUO2-04T-C01) so that multiple uranium loading analyses could be performed. This allowed for confirmation of the analysis precision. Riffling ensured that no preferential size or weight distribution was introduced in the smaller subsamples and that the three particle populations were representative of the original.

3.1 AVERAGE PARTICLE WEIGHT

Before initiating the uranium-loading analysis, uranium-loading subsample ORNL-DUO2-04T-A01 was riffled into ten temporary particle-weight subsamples. Five of these were weighed, imaged, and the particles in the images counted to determine the average particle weight. This information was needed to determine the number of particles in each uranium-loading analysis and LBL sample. Table 3-2 shows the data report form (DRF) with the data from this particle weight analysis. The mean of the average particle weights determined from the five measured particle-weight subsamples was 1.345E-3 g, with a standard error in the mean of 3.0E-6 g. After particle weight analysis, the particle-weight subsamples were recombined to reconstitute the uranium-loading subsample, ORNL-DUO2-04T-A01.

Table 3-2. Data report form for average particle weight of representative sublots

Data Report Form DRF-22: Estimation of Average Particle Weight

Procedure:	AGR-CHAR-DAM-22 Rev. 2
Operator:	Hunn and Cooley
Particle sample ID:	ORNL-DUO2-04T-A01
Particle sample description:	GIF LBL Round-Robin Representative Sublot
Filename:	\\mc-agr\AGR\ParticleWeight\W18042501_DRF22R2.xls

	Sample 1	Sample 2	Sample 3	Sample 4	Sample 5
Weight of particles (g):	0.2655	0.2764	0.3011	0.3068	0.2997
Number of particles:	198	206	222	229	223
Average weight/particle (g):	1.341E-03	1.342E-03	1.356E-03	1.340E-03	1.344E-03

Mean average weight/particle (g):	1.345E-03
Standard deviation in average weight/particle (g):	6.8E-06
Standard error in mean average weight/particle (g):	3.0E-06

Comments

ORNL-DUO2-04T-A01 was riffled into 10 temporary sub-samples for determination of average particle weight.

3.2 AVERAGE URANIUM LOADING

Uranium-loading analyses of the three subsamples riffled from representative sublot ORNL-DUO2-04T (ORNL-DUO2-04T-A01, ORNL-DUO2-04T-B01, and ORNL-DUO2-04T-C01) were performed according to the procedure described in Section 2.2. Table 3-3 shows the results of the analyses. The mean of the average uranium loading per particle determined for the three samples was 5.984E-4 g U, with a standard error in the mean of 5.4E-7 g U. Good agreement was observed among the three uranium-loading subsamples' measured values, and <0.08% of the total uranium weight was measured in the second leach for all subsamples, confirming the near-complete leaching of the accessible uranium in each subsample. After the second leach to dissolve any accessible uranium, the SiC fragments remaining in each vessel were surveyed for uranium activity, and none was detected, which indicated that there was negligible uranium not dissolved in the acid leachates.

Table 3-3. Data report form for average uranium loading of representative sublots

Data Report Form DRF-35: Fuel Particle Uranium Loading

Procedure:	AGR-CHAR-DAM-35 Rev. 0
Operator:	Fred Montgomery
Particle lot ID:	ORNL-DUO2-04T
Particle lot description:	GIF LBL Round-Robin Representative Sublot
Filename:	\\mc-agr\AGR\UraniumLoading\ORNL-DUO2-04T_DRF35R0.xls

Mean average weight per particle (g):	1.345E-03
Standard error in mean average weight per particle (g):	3.0E-06
Standard deviation in mean weight per particle (g):	6.8E-06

	Sample 1		Sample 2		Sample 3	
	Leach 1	Leach 2	Leach 1	Leach 2	Leach 1	Leach 2
Particle sample ID:	ORNL-DUO2-04T-A01		ORNL-DUO2-04T-B01		ORNL-DUO2-04T-C01	
Weight of particles:	3.2853 ± 0.0002		3.3906 ± 0.0002		3.3205 ± 0.0002	
Approximate number of particles:	2443		2522		2470	
Uncertainty in number of particles:	12		13		12	
Acid leach sample ID:	U18050201	U18050301	U18050202	U18050302	U18050203	U18050303
Radiochemical laboratory analysis number:	18300-001	18300-005	18300-002	18300-006	18300-003	18300-007
Weight U in leach (mg):	1.461E+03	6.88E-01	1.506E+03	1.09E+00	1.480E+03	3.85E-01
Uncertainty in weight U in leach (mg):	6.3E+00	1.4E-03	5.0E+00	2.2E-03	2.2E-01	7.7E-04
Total weight U in sample (mg):	1.462E+03		1.507E+03		1.480E+03	
Average weight U per particle (mg):	5.982E-01		5.976E-01		5.994E-01	
Uncertainty in average weight U per particle (mg):	4.0E-03		3.6E-03		3.0E-03	

Mean average uranium loading per particle (g):	5.984E-04
Standard error in mean average uranium loading per particle (g):	5.4E-07
Standard deviation in mean uranium loading per particle (g):	9.4E-07

Comments
Average of three Davies-Gray titrations used for the Leach 1 samples and single ICP-MS analyses used for the Leach 2 measurements. The average weight percent of ^{235}U in the three subsamples was 0.422±0.005%.

3.3 LEACH-BURN-LEACH ANALYSIS

For LBL analysis of the representative sublots, a blank sample of high-purity, 70% concentrated nitric acid was analyzed along with the three representative sublots of TRISO particles provided by INET. As described in Section 2.1, each representative sublot was subjected to a first and second 24 h preburn leach in boiling acid and a first and second 24 h postburn leach in boiling acid. The acid from each hot acid leach was separated from the solids by decanting and centrifuging, and this acid along with two subsequent cold acid rinses made up the leachate solution from which an aliquot was taken for ICP-MS to measure the concentrations of uranium and various impurities. The masses in each leachate were calculated from the measured concentrations and total leachate volumes. Before the burn and at the end of the LBL process, the solids were rinsed with water to remove residual acid and the collected rinsate was also analyzed with ICP-MS. The water rinsate analysis confirmed that dissolved elements were adequately included in the acid leachates collected prior to the water rinses. The data presented below do not include the data from the analyses of the water rinsates, because the masses in the rinsates were insignificant with respect to the masses in the leachates.

Table 3-4 shows results from the first and second preburn leaches of the three representative sublots, as well as what was measured in the associated blanks processed at the same time as the sublots. Values reported in the table are the masses determined to be in each leachate (i.e., measured concentration in aliquot multiplied by the total volume of leachate). Masses listed are for uranium and various impurities typically specified for TRISO fuel fabrication quality control (QC). The amounts of uranium in the leachates are also presented in terms of the particle equivalents of uranium, which were calculated by dividing the grams of uranium in the leachate by the average grams of uranium per particle (5.984E-4 g U per particle from Table 3-3). The first and second preburn leach data are presented in Table 3-4 as less-than values if the concentration of the element in the analyzed aliquot was unmeasurable because it was below the MDL. For the measurable first and second preburn leach data reported in Table 3-4, the estimated uncertainty in each reported mass was about 10%, and this uncertainty was dominated by the uncertainty in the ICP-MS measurement of the concentration in the aliquot.

The combined preburn leach data included at the bottom of Table 3-4 are presented as either single values or a range of values. If the concentration of an element was above the MDL in both the first and second leaches, then the masses of that element in each leachate were summed and the sum is reported as a single value in Table 3-4. If the concentration of an element was below the MDL in the first and/or second leach, then two summed masses for that element were calculated when combining the first and second leach data, in which the lower value was the sum with each unmeasurable concentration assumed to be equal to zero (i.e., its minimum possible value), and the upper value was the sum with each unmeasurable concentration assumed to be equal to the MDL (i.e., its maximum possible value). These two values are reported in Table 3-4 as a possible range for the combined mass of that element in the preburn leachates.

Table 3-4. Results from preburn leaching of representative sublots: grams before blank subtraction

	Preburn Leach of Representative Sublots from INET			BLANK
	ORNL-DUO2-01T	ORNL-DUO2-02T	ORNL-DUO2-03T	
Sample Weight (g)	41.8176 ± 0.0002	41.3057 ± 0.0002	38.9239 ± 0.0002	
Number of Particles	31102 ± 156	30721 ± 154	28950 ± 146	
	First Preburn Leach Data (before blank subtraction)			
Uranium (U) in leachate (g)	2.31E-07	2.21E-07	5.39E-06	5.25E-08
Particle equivalents of U in leachate	**0.00039**	**0.00037**	**0.00901**	**0.00009**
Aluminum (Al) in leachate (g)	1.99E-05	2.20E-05	2.66E-05	1.36E-05
Calcium (Ca) in leachate (g)	7.32E-05	4.38E-05	4.50E-05	1.83E-05
Titanium (Ti) in leachate (g)	9.42E-07	8.16E-07	6.96E-07	1.31E-06
Vanadium (V) in leachate (g)	6.32E-08	6.30E-08	5.56E-08	5.73E-08
Chromium (Cr) in leachate (g)	1.85E-06	2.42E-06	2.54E-06	7.97E-07
Manganese (Mn) in leachate (g)	1.02E-06	7.14E-07	6.55E-07	1.80E-07
Iron (Fe) in leachate (g)	2.67E-05	4.63E-05	2.78E-05	1.49E-05
Cobalt (Co) in leachate (g)	3.11E-08	3.53E-08	2.82E-06	4.05E-09
Nickel (Ni) in leachate (g)	1.33E-06	1.28E-06	5.20E-06	< 8.3E-07
	Second Preburn Leach Data (before blank subtraction)			
Uranium (U) in leachate (g)	2.91E-08	4.53E-08	2.52E-07	7.06E-08
Particle equivalents of U in leachate	**0.00005**	**0.00008**	**0.00042**	**0.00012**
Aluminum (Al) in leachate (g)	1.14E-05	1.29E-05	1.32E-05	1.06E-05
Calcium (Ca) in leachate (g)	< 1.6E-05	< 1.6E-05	2.34E-05	2.09E-05
Titanium (Ti) in leachate (g)	3.84E-07	3.44E-07	5.94E-07	3.44E-07
Vanadium (V) in leachate (g)	< 2.2E-08	< 2.1E-08	< 2.0E-08	< 2.0E-08
Chromium (Cr) in leachate (g)	7.91E-07	7.97E-07	8.12E-07	5.88E-07
Manganese (Mn) in leachate (g)	1.43E-07	1.08E-07	1.14E-07	9.02E-08
Iron (Fe) in leachate (g)	7.04E-06	9.46E-06	6.33E-06	3.16E-06
Cobalt (Co) in leachate (g)	4.26E-09	2.74E-09	1.13E-07	< 2.2E-09
Nickel (Ni) in leachate (g)	< 7.7E-07	< 7.4E-07	< 6.9E-07	1.15E-06
	Combined Preburn Leach Data (before blank subtraction)			
Uranium (U) in leachates (g)	2.60E-07	2.67E-07	5.65E-06	
Particle equivalents of U in leachates	**0.00044**	**0.00045**	**0.00943**	
Aluminum (Al) in leachates (g)	3.13E-05	3.49E-05	3.98E-05	
Calcium (Ca) in leachates (g)	7.32E-05 – 8.95E-05	4.38E-05 – 5.94E-05	6.84E-05	
Titanium (Ti) in leachates (g)	1.33E-06	1.16E-06	1.29E-06	
Vanadium (V) in leachates (g)	6.32E-08 – 8.53E-08	6.30E-08 – 8.41E-08	5.56E-08 – 7.54E-08	
Chromium (Cr) in leachates (g)	2.65E-06	3.22E-06	3.35E-06	
Manganese (Mn) in leachates (g)	1.16E-06	8.22E-07	7.69E-07	
Iron (Fe) in leachates (g)	3.37E-05	5.57E-05	3.41E-05	
Cobalt (Co) in leachates (g)	3.54E-08	3.81E-08	2.93E-06	
Nickel (Ni) in leachates (g)	1.33E-06 – 2.11E-06	1.28E-06 – 2.02E-06	5.20E-06 – 5.90E-06	

Note: Less-than values (displayed in gray) indicate the concentration in the aliquot was below the MDL.
Note: The one-sigma uncertainties in the measurable data from the first and second leaches were estimated to be ~10%, based on multiple ICP-MS measurements of standard samples. However, values are presented with additional significant figures, in some cases, for ease of comparison between leaches.
Note: Presented ranges incorporate the MDL as described in the text.

Table 3-5 shows the masses of uranium and QC-relevant impurities determined to be in the leachates from the first and second postburn leaches of the three representative sublots, as well as what was measured in the high-purity acid postburn leach blanks. The results from the first and second postburn leaches are presented in the same way as the preburn leach data in Table 3-4, as described in the preceding two paragraphs. Compared with the preburn leach data, there were more cases in the postburn leach data in which the concentration of a QC-relevant impurity was below the MDL. Reported ranges for the combined data with a lower bound of zero indicate that the aliquots from both the first and second postburn leaches contained concentrations below the MDL.

Table 3-5. Results from postburn leaching of representative sublots: grams before blank subtraction

	Postburn Leach of Representative Sublots from INET			BLANK
	ORNL-DUO2-01T	ORNL-DUO2-02T	ORNL-DUO2-03T	
Sample Weight (g)	41.8176 ± 0.0002	41.3057 ± 0.0002	38.9239 ± 0.0002	
Number of Particles	31102 ± 156	30721 ± 154	28950 ± 146	
	First Postburn Leach Data (before blank subtraction)			
Uranium (U) in leachate (g)	8.97E-07	2.27E-07	1.81E-07	3.54E-08
Particle equivalents of U in leachate	**0.00150**	**0.00038**	**0.00030**	**0.00006**
Aluminum (Al) in leachate (g)	1.23E-05	1.08E-05	9.74E-06	1.06E-05
Calcium (Ca) in leachate (g)	2.68E-05	2.61E-05	< 1.2E-05	1.49E-05
Titanium (Ti) in leachate (g)	2.45E-07	1.54E-07	1.13E-07	< 1.1E-07
Vanadium (V) in leachate (g)	< 1.7E-08	4.33E-08	3.10E-08	< 1.8E-08
Chromium (Cr) in leachate (g)	8.04E-07	7.28E-07	1.84E-06	5.64E-07
Manganese (Mn) in leachate (g)	1.98E-07	1.30E-07	1.64E-07	8.82E-08
Iron (Fe) in leachate (g)	1.12E-05	1.28E-05	1.55E-05	2.62E-06
Cobalt (Co) in leachate (g)	6.03E-09	1.07E-08	8.88E-09	< 2.0E-09
Nickel (Ni) in leachate (g)	< 6.1E-07	< 6.1E-07	< 5.9E-07	< 6.4E-07
	Second Postburn Leach Data (before blank subtraction)			
Uranium (U) in leachate (g)	3.14E-08	3.16E-08	1.46E-08	6.30E-09
Particle equivalents of U in leachate	**0.00005**	**0.00005**	**0.00002**	**0.00001**
Aluminum (Al) in leachate (g)	1.01E-05	6.34E-06	1.02E-05	1.87E-05
Calcium (Ca) in leachate (g)	3.29E-05	1.77E-05	< 1.2E-05	1.91E-04
Titanium (Ti) in leachate (g)	< 1.1E-07	< 1.0E-07	< 1.0E-07	3.54E-07
Vanadium (V) in leachate (g)	< 1.7E-08	< 1.7E-08	< 1.7E-08	< 1.6E-08
Chromium (Cr) in leachate (g)	8.00E-07	1.53E-07	1.30E-06	1.52E-06
Manganese (Mn) in leachate (g)	4.59E-08	6.10E-08	7.49E-08	1.76E-07
Iron (Fe) in leachate (g)	2.14E-06	2.47E-06	6.79E-06	1.00E-05
Cobalt (Co) in leachate (g)	< 1.9E-09	2.44E-09	2.21E-09	4.02E-09
Nickel (Ni) in leachate (g)	< 6.1E-07	< 6.0E-07	< 5.8E-07	< 5.7E-07
	Combined Postburn Leach Data (before blank subtraction)			
Uranium (U) in leachates (g)	9.28E-07	2.58E-07	1.95E-07	
Particle equivalents of U in leachates	**0.00155**	**0.00043**	**0.00033**	
Aluminum (Al) in leachates (g)	2.24E-05	1.72E-05	2.00E-05	
Calcium (Ca) in leachates (g)	5.97E-05	4.38E-05	0 – 2.48E-05	
Titanium (Ti) in leachates (g)	2.45E-07 – 3.50E-07	1.54E-07 – 2.58E-07	1.13E-07 – 2.14E-07	
Vanadium (V) in leachates (g)	0 – 3.46E-08	4.33E-08 – 6.03E-08	3.10E-08 – 4.75E-08	
Chromium (Cr) in leachates (g)	1.60E-06	8.81E-07	3.13E-06	
Manganese (Mn) in leachates (g)	2.44E-07	1.91E-07	2.39E-07	
Iron (Fe) in leachates (g)	1.34E-05	1.53E-05	2.23E-05	
Cobalt (Co) in leachates (g)	6.03E-09 – 7.95E-09	1.31E-08	1.11E-08	
Nickel (Ni) in leachates (g)	0 – 1.21E-06	0 – 1.21E-06	0 – 1.17E-06	

Note: See footnotes in Table 3-4.

The amounts of uranium and QC-relevant impurities in the sublot leachates were generally low, but above the MDLs in most cases. However, in several cases, the masses in the sublot leachates were not significantly higher (and sometimes lower) than those in the leachates from the high-purity acid blanks. Values measured in the blanks may have come from contamination in the LBL glassware, ICP-MS analytical equipment, and/or airborne dust in the laboratory (calcium is a primary constituent in the dust

from the gypsum ceiling tiles, while iron and chromium are prevalent in particulates expelled from the galvanized ductwork). Significant contribution from contamination in the LBL glassware was unlikely if the mass of a QC-relevant impurity in the control blank was higher in the second leach than in the first leach. Measured values close to the MDL can also be expected to have higher than the estimated 10% uncertainty in most values. To consider the measured values with respect to the possible background levels indicated by the blanks, Table 3-6 and Table 3-7 present the data from Table 3-4 and Table 3-5 after subtraction of the associated blank data.

Table 3-6. Results from preburn leaching of representative sublots: grams after blank subtraction

	Preburn Leach of Representative Sublots from INET		
	ORNL-DUO2-01T	ORNL-DUO2-02T	ORNL-DUO2-03T
Sample Weight (g)	41.8176 ± 0.0002	41.3057 ± 0.0002	38.9239 ± 0.0002
Number of Particles	31102 ± 156	30721 ± 154	28950 ± 146
	First Preburn Leach Data (after blank subtraction)		
Uranium (U) in leachate (g)	1.79E-07	1.69E-07	5.34E-06
Particle equivalents of U in leachate	**0.00030**	**0.00028**	**0.00893**
Aluminum (Al) in leachate (g)	6.30E-06	8.42E-06	1.30E-05
Calcium (Ca) in leachate (g)	5.49E-05	2.55E-05	2.67E-05
Titanium (Ti) in leachate (g)	0	0	0
Vanadium (V) in leachate (g)	5.96E-09	5.72E-09	0
Chromium (Cr) in leachate (g)	1.06E-06	1.62E-06	1.74E-06
Manganese (Mn) in leachate (g)	8.37E-07	5.34E-07	4.75E-07
Iron (Fe) in leachate (g)	1.17E-05	3.13E-05	1.28E-05
Cobalt (Co) in leachate (g)	2.71E-08	3.13E-08	2.82E-06
Nickel (Ni) in leachate (g)	5.02E-07 – 1.33E-06	4.53E-07 – 1.28E-06	4.37E-06 – 5.20E-06
	Second Preburn Leach Data (after blank subtraction)		
Uranium (U) in leachate (g)	0	0	1.81E-07
Particle equivalents of U in leachate	**0**	**0**	**0.00030**
Aluminum (Al) in leachate (g)	8.17E-07	2.33E-06	2.63E-06
Calcium (Ca) in leachate (g)	0	0	2.46E-06
Titanium (Ti) in leachate (g)	4.06E-08	7.00E-11	2.50E-07
Vanadium (V) in leachate (g)	0 – 2.21E-08	0 – 2.11E-08	0 – 1.98E-08
Chromium (Cr) in leachate (g)	2.03E-07	2.09E-07	2.24E-07
Manganese (Mn) in leachate (g)	5.25E-08	1.75E-08	2.35E-08
Iron (Fe) in leachate (g)	3.88E-06	6.30E-06	3.17E-06
Cobalt (Co) in leachate (g)	2.05E-09 – 4.26E-09	5.31E-10 – 2.74E-09	1.10E-07 – 1.13E-07
Nickel (Ni) in leachate (g)	0	0	0
	Combined Preburn Leach Data (after blank subtraction)		
Uranium (U) in leachates (g)	1.79E-07	1.69E-07	5.52E-06
Particle equivalents of U in leachates	**0.00030**	**0.00028**	**0.00923**
Aluminum (Al) in leachates (g)	7.12E-06	1.07E-05	1.56E-05
Calcium (Ca) in leachates (g)	5.49E-05	2.55E-05	2.92E-05
Titanium (Ti) in leachates (g)	4.06E-08	7.00E-11	2.50E-07
Vanadium (V) in leachates (g)	5.96E-09 – 2.80E-08	5.72E-09 – 2.68E-08	0 – 1.98E-08
Chromium (Cr) in leachates (g)	1.26E-06	1.83E-06	1.97E-06
Manganese (Mn) in leachates (g)	8.89E-07	5.51E-07	4.98E-07
Iron (Fe) in leachates (g)	1.56E-05	3.76E-05	1.60E-05
Cobalt (Co) in leachates (g)	2.91E-08 – 3.13E-08	3.18E-08 – 3.40E-08	2.93E-06 – 2.93E-06
Nickel (Ni) in leachates (g)	5.02E-07 – 1.33E-06	4.53E-07 – 1.28E-06	4.37E-06 – 5.20E-06

Note: See footnotes in Table 3-4.

The blank subtraction for Table 3-6 and Table 3-7 was done using the masses in each leachate with the assumption that the introduction of the background contamination was independent of the size of the sample or volume of the leachate. The first and second leach data after blank subtraction are presented as either single values or a range of values. If the mass of an element in the blank leachate was greater than the mass in the sublot leachate, then the blank-subtracted value was reported as zero. Otherwise, if the concentration of an element was above the MDL in both associated sublot and blank aliquots, then the

blank leachate mass was subtracted from the sublot leachate mass, and the difference reported as a single value. If the concentration of an element was below the MDL in the sublot or blank aliquot, then a range of sublot minus blank values were reported. The lower end of the range was the mass difference assuming zero for the sublot, if it was unmeasurable, and assuming the MDL for the blank concentration, if it was unmeasurable (if the calculated value was negative, then the lower limit was reported as zero). The upper end of the range was the mass difference assuming the MDL for the sublot concentration, if it was unmeasurable, and assuming zero for the blank, if it was unmeasurable. These two values are reported in Table 3-6 and Table 3-7 as a possible range for the total blank-subtracted mass of that element leached from the sublot. The combined preburn leach and postburn leach data after blank subtraction are also presented as either single values or a range of values. If the associated first and second leach data are presented as single values, then these were added and presented as a single combined value. If either was presented as a range, then the minimum possible values were summed to determine the lower end of the combined range and the maximum possible values were summed to determine the upper end of the combined range.

Table 3-7. Results from postburn leaching of representative sublots: grams after blank subtraction

	Postburn Leach of Representative Sublots from INET		
	ORNL-DUO2-01T	ORNL-DUO2-02T	ORNL-DUO2-03T
Sample Weight (g)	41.8176 ± 0.0002	41.3057 ± 0.0002	38.9239 ± 0.0002
Number of Particles	31102 ± 156	30721 ± 154	28950 ± 146
	First Postburn Leach Data (after blank subtraction)		
Uranium (U) in leachate (g)	8.61E-07	1.91E-07	1.45E-07
Particle equivalents of U in leachate	**0.00144**	**0.00032**	**0.00024**
Aluminum (Al) in leachate (g)	1.73E-06	2.73E-07	0
Calcium (Ca) in leachate (g)	1.19E-05	1.12E-05	0
Titanium (Ti) in leachate (g)	1.34E-07 – 2.45E-07	4.36E-08 – 1.54E-07	1.77E-09 – 1.13E-07
Vanadium (V) in leachate (g)	0 – 1.73E-08	2.52E-08 – 4.33E-08	1.28E-08 – 3.10E-08
Chromium (Cr) in leachate (g)	2.39E-07	1.63E-07	1.27E-06
Manganese (Mn) in leachate (g)	1.10E-07	4.19E-08	7.61E-08
Iron (Fe) in leachate (g)	8.60E-06	1.02E-05	1.29E-05
Cobalt (Co) in leachate (g)	4.01E-09 – 6.03E-09	8.67E-09 – 1.07E-08	6.86E-09 – 8.88E-09
Nickel (Ni) in leachate (g)	0 – 6.08E-07	0 – 6.14E-07	0 – 5.89E-07
	Second Postburn Leach Data (after blank subtraction)		
Uranium (U) in leachate (g)	2.51E-08	2.53E-08	8.30E-09
Particle equivalents of U in leachate	**0.00004**	**0.00004**	**0.00001**
Aluminum (Al) in leachate (g)	0	0	0
Calcium (Ca) in leachate (g)	0	0	0
Titanium (Ti) in leachate (g)	0	0	0
Vanadium (V) in leachate (g)	0 – 1.73E-08	0 – 1.70E-08	0 – 1.66E-08
Chromium (Cr) in leachate (g)	0	0	0
Manganese (Mn) in leachate (g)	0	0	0
Iron (Fe) in leachate (g)	0	0	0
Cobalt (Co) in leachate (g)	0	0	0
Nickel (Ni) in leachate (g)	0 – 6.05E-07	0 – 5.95E-07	0 – 5.80E-07
	Combined Postburn Leach Data (after blank subtraction)		
Uranium (U) in leachates (g)	8.86E-07	2.17E-07	1.53E-07
Particle equivalents of U in leachates	**0.00148**	**0.00036**	**0.00026**
Aluminum (Al) in leachates (g)	1.73E-06	2.73E-07	0
Calcium (Ca) in leachates (g)	1.19E-05	1.12E-05	0
Titanium (Ti) in leachates (g)	1.34E-07 – 2.45E-07	4.36E-08 – 1.54E-07	1.77E-09 – 1.13E-07
Vanadium (V) in leachates (g)	0 – 3.46E-08	2.52E-08 – 6.03E-08	1.28E-08 – 4.75E-08
Chromium (Cr) in leachates (g)	2.39E-07	1.63E-07	1.27E-06
Manganese (Mn) in leachates (g)	1.10E-07	4.19E-08	7.61E-08
Iron (Fe) in leachates (g)	8.60E-06	1.02E-05	1.29E-05
Cobalt (Co) in leachates (g)	4.01E-09 – 6.03E-09	8.67E-09 – 1.07E-08	6.86E-09 – 8.88E-09
Nickel (Ni) in leachates (g)	0 – 1.21E-06	0 – 1.21E-06	0 – 1.17E-06

Note: See footnotes in Table 3-4.

While the sublot sizes were nearly equal, to rigorously compare results between sublots and allow for averaging, the mass values were converted to parts per million (ppm) by dividing by the sample weights. Table 3-8 presents the ppm values before blank subtraction associated with the combined preburn leach mass data from Table 3-4 and the combined postburn leach mass data from Table 3-5. Table 3-9 presents the ppm values after blank subtraction associated with the combined preburn leach mass data from Table 3-6 and the combined postburn leach mass data from Table 3-7. Ranges shown in Table 3-8 and Table 3-9 incorporate the same MDL combination rules as were applied to the mass data tables.

Table 3-8. Representative sublot leach-burn-leach summary: ppm before blank subtraction

	Leach-Burn-Leach Analysis of Representative Sublots from INET			Average
	ORNL-DUO2-01T	ORNL-DUO2-02T	ORNL-DUO2-03T	
Sample Weight (g)	41.8176 ± 0.0002	41.3057 ± 0.0002	38.9239 ± 0.0002	
Number of Particles	31102 ± 156	30721 ± 154	28950 ± 146	
	Combined Preburn Leach Data (before blank subtraction)			
Uranium (U) in leachates (ppm)	0.00623	0.00646	0.14504	0.05258
Particle equivalents of U in leachates	**0.00044**	**0.00045**	**0.00943**	**0.00344**
Aluminum (Al) in leachates (ppm)	0.74856	0.84568	1.02187	0.87204
Calcium (Ca) in leachates (ppm)	1.74950 – 2.14132	1.06039 – 1.43923	1.75713	1.52234 – 1.77923
Titanium (Ti) in leachates (ppm)	0.03173	0.02808	0.03314	0.03098
Vanadium (V) in leachates (ppm)	0.00151 – 0.00204	0.00153 – 0.00204	0.00143 – 0.00194	0.00149 – 0.00200
Chromium (Cr) in leachates (ppm)	0.06325	0.07784	0.08609	0.07573
Manganese (Mn) in leachates (ppm)	0.02773	0.01989	0.01975	0.02246
Iron (Fe) in leachates (ppm)	0.80588	1.34898	0.87647	1.01044
Cobalt (Co) in leachates (ppm)	0.00085	0.00092	0.07533	0.02570
Nickel (Ni) in leachates (ppm)	0.03188 – 0.05035	0.03109 – 0.04895	0.13361 – 0.15145	0.06552 – 0.08358
	Combined Postburn Leach Data (before blank subtraction)			
Uranium (U) in leachates (ppm)	0.02219	0.00625	0.00501	0.01115
Particle equivalents of U in leachates	**0.00155**	**0.00043**	**0.00033**	**0.00077**
Aluminum (Al) in leachates (ppm)	0.53451	0.41584	0.51348	0.48794
Calcium (Ca) in leachates (ppm)	1.42749	1.05919	0 – 0.63716	0.82889 – 1.04128
Titanium (Ti) in leachates (ppm)	0.00586 – 0.00838	0.00374 – 0.00625	0.00289 – 0.00549	0.00416 – 0.00671
Vanadium (V) in leachates (ppm)	0 – 0.00083	0.00105 – 0.00146	0.00080 – 0.00122	0.00061 – 0.00117
Chromium (Cr) in leachates (ppm)	0.03836	0.02132	0.08053	0.04674
Manganese (Mn) in leachates (ppm)	0.00583	0.00463	0.00615	0.00553
Iron (Fe) in leachates (ppm)	0.31956	0.37023	0.57217	0.42065
Cobalt (Co) in leachates (ppm)	0.00014 – 0.00019	0.00032	0.00028	0.00025 – 0.00026
Nickel (Ni) in leachates (ppm)	0 – 0.02900	0 – 0.02927	0 – 0.03004	0 – 0.02944
	Combined Leach-Burn-Leach Data (before blank subtraction)			
Uranium (U) in leachates (ppm)	0.02842	0.01271	0.15006	0.06373
Particle equivalents of U in leachates	**0.00199**	**0.00088**	**0.00976**	**0.00421**
Aluminum (Al) in leachates (ppm)	1.28307	1.26152	1.53535	1.35998
Calcium (Ca) in leachates (ppm)	3.17699 – 3.56881	2.11957 – 2.49842	1.75713 – 2.39430	2.35123 – 2.82051
Titanium (Ti) in leachates (ppm)	0.03759 – 0.04011	0.03182 – 0.03433	0.03603 – 0.03862	0.03514 – 0.03769
Vanadium (V) in leachates (ppm)	0.00151 – 0.00287	0.00257 – 0.00350	0.00222 – 0.00316	0.00210 – 0.00317
Chromium (Cr) in leachates (ppm)	0.10161	0.09916	0.16662	0.12246
Manganese (Mn) in leachates (ppm)	0.03356	0.02452	0.02590	0.02799
Iron (Fe) in leachates (ppm)	1.12544	1.71921	1.44863	1.43109
Cobalt (Co) in leachates (ppm)	0.00099 – 0.00104	0.00124	0.07562	0.02595 – 0.02596
Nickel (Ni) in leachates (ppm)	0.03188 – 0.07935	0.03109 – 0.07822	0.13361 – 0.18149	0.06552 – 0.11302

Note: See footnotes in Table 3-4.

For all three representative sublots, the particle equivalents of uranium in the preburn leachates were well below what would be detected if particles with exposed-kernel defects were present. Therefore, the small masses of uranium that were measured can be presumed to be uranium contamination as discussed in Sections 1.1 and 2.1. Table 3-4 and Table 3-6 show that the masses of uranium dissolved in the first preburn leachates were measurably above the blank in all the representative sublots. The uranium contamination detected in the preburn analysis of Sublot ORNL-DUO2-03T, 0.145 ppm before blank

subtraction (Table 3-8) and 0.141 ppm after blank subtraction (Table 3-9), was significantly higher than the other two sublots (~0.004 after blank subtraction), but less than 1% of the uranium in an average particle (<0.01 particle equivalents of uranium). This amount of uranium is not indicative of the presence of a defective particle, especially given the inconsequential additional uranium detected during the second preburn leach and postburn leaches of this sample, which would have been higher in the case of a partially leached kernel. Because these three sublots were riffled from the same particle production lot, it is likely that the elevated uranium measured in Sublot ORNL-DUO2-03T was associated with localized contamination in one or more of the particles in the sublot. The mass of uranium dissolved in the second preburn leachate of sublot ORNL-DUO2-03T was a few percent of what was measured in the first leachate, and this small residual value remaining after the first hot leach and acid rinses is not unusual. The masses of uranium measured in the second preburn leachates of the other two sublots were less than that in the associated blank.

Table 3-9. Representative sublot leach-burn-leach summary: ppm after blank subtraction

	Leach-Burn-Leach Analysis of Representative Sublots from INET			Average
	ORNL-DUO2-01T	ORNL-DUO2-02T	ORNL-DUO2-03T	
Sample Weight (g)	41.8176 ± 0.0002	41.3057 ± 0.0002	38.9239 ± 0.0002	
Number of Particles	31102 ± 156	30721 ± 154	28950 ± 146	
	Combined Preburn Leach Data (after blank subtraction)			
Uranium (U) in leachates (ppm)	0.00428	0.00409	0.14188	0.05008
Particle equivalents of U in leachates	**0.00030**	**0.00028**	**0.00923**	**0.00327**
Aluminum (Al) in leachates (ppm)	0.17021	0.26017	0.40053	0.27697
Calcium (Ca) in leachates (ppm)	1.31210	0.61757	0.74914	0.89294
Titanium (Ti) in leachates (ppm)	0.00097	0.00000	0.00642	0.00246
Vanadium (V) in leachates (ppm)	0.00014 – 0.00067	0.00014 – 0.00065	0 – 0.00051	0.00009 – 0.00061
Chromium (Cr) in leachates (ppm)	0.03012	0.04430	0.05050	0.04164
Manganese (Mn) in leachates (ppm)	0.02126	0.01335	0.01281	0.01580
Iron (Fe) in leachates (ppm)	0.37306	0.91080	0.41147	0.56511
Cobalt (Co) in leachates (ppm)	0.00070 – 0.00075	0.00077 – 0.00082	0.07517 – 0.07523	0.02555 – 0.02560
Nickel (Ni) in leachates (ppm)	0.01201 – 0.03188	0.01097 – 0.03109	0.11227 – 0.13361	0.04508 – 0.06552
	Combined Postburn Leach Data (after blank subtraction)			
Uranium (U) in leachates (ppm)	0.02120	0.00524	0.00394	0.01013
Particle equivalents of U in leachates	**0.00148**	**0.00036**	**0.00026**	**0.00070**
Aluminum (Al) in leachates (ppm)	0.04140	0.00660	0	0.01600
Calcium (Ca) in leachates (ppm)	0.28396	0.27014	0	0.18470
Titanium (Ti) in leachates (ppm)	0.00321 – 0.00586	0.00106 – 0.00374	0.00005 – 0.00289	0.00144 – 0.00416
Vanadium (V) in leachates (ppm)	0 – 0.00083	0.00061 – 0.00146	0.00033 – 0.00122	0.00031 – 0.00117
Chromium (Cr) in leachates (ppm)	0.00572	0.00395	0.03273	0.01414
Manganese (Mn) in leachates (ppm)	0.00262	0.00102	0.00196	0.00186
Iron (Fe) in leachates (ppm)	0.20577	0.24704	0.33061	0.26114
Cobalt (Co) in leachates (ppm)	0.00010 – 0.00014	0.00021 – 0.00026	0.00018 – 0.00023	0.00016 – 0.00021
Nickel (Ni) in leachates (ppm)	0 – 0.02900	0 – 0.02927	0 – 0.03004	0 – 0.02944
	Combined Leach-Burn-Leach Data (after blank subtraction)			
Uranium (U) in leachates (ppm)	0.02547	0.00933	0.14583	0.06021
Particle equivalents of U in leachates	**0.00178**	**0.00064**	**0.00949**	**0.00397**
Aluminum (Al) in leachates (ppm)	0.21161	0.26677	0.40053	0.29297
Calcium (Ca) in leachates (ppm)	1.59607	0.88770	0.74914	1.07764
Titanium (Ti) in leachates (ppm)	0.00418 – 0.00683	0.00106 – 0.00374	0.00646 – 0.00931	0.00390 – 0.00663
Vanadium (V) in leachates (ppm)	0.00014 – 0.00150	0.00075 – 0.00211	0.00033 – 0.00173	0.00041 – 0.00178
Chromium (Cr) in leachates (ppm)	0.03585	0.04826	0.08323	0.05578
Manganese (Mn) in leachates (ppm)	0.02388	0.01436	0.01476	0.01767
Iron (Fe) in leachates (ppm)	0.57883	1.15784	0.74208	0.82625
Cobalt (Co) in leachates (ppm)	0.00079 – 0.00089	0.00098 – 0.00108	0.07535 – 0.07546	0.02571 – 0.02581
Nickel (Ni) in leachates (ppm)	0.01201 – 0.06088	0.01097 – 0.06035	0.11227 – 0.16365	0.04508 – 0.09496

Note: See footnotes in Table 3-4.

For all three representative sublots, the particle equivalents of uranium measured in the postburn leachates were well below what would be detected if particles with defective SiC were present. Therefore, as for the preburn leach results, the small masses of uranium that were dissolved during the postburn leaching can be presumed to be uranium contamination. Table 3-5 and Table 3-7 show that the masses of uranium dissolved in the first postburn leaches were measurably above the blank in all the representative sublots. The uranium contamination detected in the postburn analysis of Sublot ORNL-DUO2-01T, 0.022 ppm before blank subtraction (Table 3-8) and 0.021 ppm after blank subtraction (Table 3-9), was roughly 4× higher than the other two sublots, but less than 0.002 particle equivalents of uranium, so not related to SiC failure. Again, this most likely indicated localized contamination, although in this case the contamination was not soluble until after oxidation occurred during the burn phase. Perhaps the contamination was a small kernel fragment sequestered within the OPyC layer of one particle, as such can sometimes occur if kernel debris is generated by kernel-kernel collision during loading or fluidization of the bare kernels.

Overall, the LBL data for uranium indicated that a small amount of uranium was present outside of the TRISO particle SiC coating layers. This is not unexpected and can be explained by pick up of uranium contamination present within the fluidized-bed chemical vapor deposition (FB-CVD) coating furnace. When uranium-bearing kernels are first introduced into the coating furnace, they are uncoated, and uranium at the surface of the kernels may react with carbon in the furnace as the kernels are heated to the deposition temperature of the first layer (typically around 1400°C). Such uranium-contaminated carbon may be transferred to the coating layers as they are deposited. The average uranium contamination measured in the three representative sublots analyzed by ORNL was 0.064 ppm before blank subtraction (Table 3-8) and 0.060 ppm after blank subtraction (Table 3-9), which equates to ~1.4E-7 grams uranium contamination per gram uranium in the sample. To provide perspective, this amount of uranium contamination is well below the AGR program specified upper limit of ≤1.0E-5 grams uranium contamination per gram uranium in a compact (Marshall 2017).

Assuming a binomial distribution, zero particles with exposed-kernel defects or SiC defects out of a total of approximately 90,773 analyzed particles in these three representative sublots gives a 95% confidence interval with an upper bound of ≤3.4E-5. While a lower upper bound on the 95% confidence interval could possibly be achieved by measuring a larger sample size if the actual exposed-kernel and SiC defect fractions in the parent lot were much lower than 3.4E-5, the results from just these three representative sublots would be sufficient to pass with 95% confidence the specified defect fractional limits of ≤5.0E-5 exposed-kernel defects and ≤1.0E-4 SiC defects allowed in compacts fabricated under the AGR program (Marshall 2017).

Considering the combined LBL data after blank-subtraction for the listed impurities shown at the bottom of Table 3-9, all measured impurities were low relative to typically specified limits, such as upper limits on the mean of <25–50 ppm for AGR fuel compacts (Marshall 2017). The predominant measured impurities were Al, Ca, and Fe, which had average combined LBL values after blank-subtraction of 0.30, 1.08, and 0.83 ppm, respectively, while all other measured impurities averaged below 0.1 ppm. Given the lack of any particles with exposed-kernel or SiC defects, measured impurities can be assumed to have been on the TRISO particle surface, in the OPyC, or to have been incorporated from external sources during the LBL analysis. Comparison of the Al, Ca, and Fe values reported in Table 3-6 and Table 3-7 for each individual leach shows that the first preburn leach was the most significant contributor to the combined LBL data after blank-subtraction reported in Table 3-9, which suggests that most of these impurities were on the surface of the TRISO or came from external sources. Table 3-4 and Table 3-5 show that Al, Ca, and Fe also had the highest masses in the blank samples, and that the blank values were often significant compared with the values measured for the three representative TRISO sublots. Therefore, the blank subtracted data should be considered to have a high fractional uncertainty. It is worth noting, however, that this high uncertainty stemming from the large fractional contribution from the blank subtraction was exacerbated by the low impurity content in the representative sublots tested, and the observed levels in the blanks would not significantly impact rejection of samples with impurity content

exceeding typically specified limits, which would be more than an order of magnitude higher than what was measured in the blanks.

Impurities of Al, Ca, and Fe can be introduced during particle handling, either prior to coating during handling of the kernels or after coating during TRISO particle upgrading and characterization. Inclusion of Ca was identified during early AGR program fabrication and traced to airborne dust particles from the gypsum ceiling tiles in the ORNL Coated Particle Fuel Development (CPFD) Laboratory. After this observation, care was taken to clean and cover operations prone to dust collection, and this reduced the inclusion of Ca in particle samples. However, pick up of airborne contaminates cannot be completely controlled for some operations without general area solutions, such as working in a clean room. Iron can come from the galvanized ductwork in the CPFD Laboratory, or from the stainless steel equipment typically used for particle upgrading and riffling. Aluminum might be introduced by Al weigh pans. However, particle handling was minimized prior to LBL of the three representative sublots by weighing the bottles containing each sample and then transferring the TRISO particles directly from the glass bottles in which they were received to the quartz flasks used for LBL.

Although measured impurities in all three sublots were very low overall, Sublot ORNL-DUO2-03T had significantly higher levels of Co and Ni, and moderately more Cr and Ti, relative to the other two sublots, which suggests the presence of discrete contamination from a steel alloy not included in the other two sublots. Most (>95%) of the Co and Ni in Sublot ORNL-DUO2-03T was detected in the first preburn leach, which indicates that these impurities were present in a readily accessible and soluble form, such as a small, included particulate.

4. ANALYSIS OF SIMULATED SAMPLES

The ORNL-designated series of seven simulated samples described in Section 1.3 and labeled ORNL-A through ORNL-G was subjected to LBL analysis as described in Section 2.1 to detect and count the number of particles in each sample that had simulated exposed-kernel defects or simulated SiC defects via analysis of leached uranium. The number of defects in each sample was expected to be zero, one, two, or four (see Section 1.3). In addition, the amounts of various trace elements in the LBL leachates were measured for comparison to the masses contained within the added coal impurity standard (NIST SRM 1632d). After each institution had completed and reported on LBL analysis of their simulated sample set at a GIF meeting, information on the population of particles with simulated defects and the masses of the added impurities was distributed to participants via a revision to ORNL/TM-2015/722 (Gerczak et al. 2022). Appendix A contains this information for simulated samples ORNL-A through ORNL-G.

The elements investigated during LBL analysis of ORNL-A through ORNL-G and discussed herein included elements typically specified for fuel fabrication QC acceptance testing (Al, Ca, Ti, V, Cr, Mn, Fe, Co, Ni, and U) and a targeted list of other elements available in the coal standard, some of which are sometimes measured during LBL of irradiated fuel (Sb, Ba, Cd, Ce, Cs, Eu, Rb, Sr, and Th). All the elements except nickel had concentrations reported in the NIST SRM 1632d documentation as either NIST certified values (high-confidence values whose uncertainties included investigation or accounting for known or suspected sources of bias) or NIST reference values (values whose uncertainties may reflect only measurement precision). The nickel concentration in the coal standard was provided as a value for information purposes only because insufficient information was available to assess the uncertainty.

As for the representative sublots discussed in Section 3.3, the simulated samples were subjected to two successive 24 h preburn leaches in boiling concentrated nitric acid followed by cold acid rinses. For each leach, the hot leach and cold rinse acids were separated from the solids by decanting and centrifuging and collected into a single volume of leachate solution for ICP-MS. The solids were then rinsed with water to remove residual acid, and the water rinsate was also analyzed. After burning in flowing air at 750°C to remove all exposed carbon, the process was repeated for the postburn leach phase. Samples ORNL-D and ORNL-G were subjected to more than two 24 h leaches during the postburn leach phase in accordance with the standard ORNL practice discussed in Section 2.1 for when uranium in a second or succeeding leachate is above the MDL and more than a significant fraction (typically determined to be 10%–20%) of the cumulative amount measured in the preceding leachate(s) in that phase. This additional leaching is done because observation of significant levels of uranium in second or succeeding leachates of a series indicate possibly incomplete leaching that would result in undercounting the number of defective particles in a sample. The feedback the second leach provides regarding the completeness of the leaching process is why a minimum of two leaches are always performed for each phase, as opposed to one longer leach.

4.1 URANIUM ANALYSIS BY LEACH-BURN-LEACH FOR DEFECT DETECTION

Table 4-1 lists the uranium measured in each leachate of the LBL analysis of simulated samples ORNL-A through ORNL-G, as well as the associated blanks, in terms of mass and particle equivalents. The particle equivalents were calculated by dividing the measured mass of dissolved uranium by the average grams of uranium per particle (7.003E-4 g), as reported by Gerczak et al. (2022). Uranium measured in the high-purity acid blanks was low compared with leachates that had significant contributions from particles with simulated defects. However, in some cases, the amounts of uranium measured in the sample leachates were only marginally higher than in the blanks, which indicates higher uncertainty in the lower measured values. As discussed in Section 3.3, uranium and other impurities measured in the blanks may come from contamination introduced during LBL or ICP-MS. The uranium values measured in the second blank leaches were consistently 10%–20% of the amounts measured in the first blank leaches, which suggests that the LBL glassware may have been a source for the observed uranium contamination. Table 4-2 shows

the uranium data after blank subtraction. However, it should be noted that the blanks provide only a rough estimate of possible background contributions to the values measured in the samples.

As discussed in Section 2.1, the presence of exposed-kernel defects and SiC defects should be indicated by near integral values in the preburn leach or postburn leach, respectively. Table 4-1 shows that the particle equivalents of uranium leached from the ORNL-B sample were negligible for every stage of the LBL and that the total uranium measured in the leachates was only 0.06% of the average uranium in one particle. In contrast, all other samples had significant quantities of uranium in at least one LBL leachate solution. Thus, ORNL-B was concluded to be the one expected round-robin sample with no simulated defects added. This conclusion was consistent with the answer key reported in Gerczak et al. (2022) and summarized in Appendix Table A-1. As listed in Appendix Table A-2, the impurity standard added to ORNL-B included 2.51±0.06E-7 g U, which accounts for 60–72% of the uranium measured in ORNL-B (4.2E-7 g before blank subtraction and 3.5E-7 g after blank subtraction).

Table 4-1. Uranium in simulated sample leachates: measured values

Uranium in leachate	Leach-Burn-Leach of Simulated Samples							BLANK ABC	BLANK DEFG [a]
	ORNL-A	ORNL-B	ORNL-C	ORNL-D	ORNL-E	ORNL-F	ORNL-G		
	First Preburn Leach Data (before blank subtraction)								
Mass (g)	1.25E-03	2.66E-07	6.54E-04	3.70E-07	5.23E-07	2.78E-03	4.55E-07	4.73E-08	2.38E-08
Part. equiv.	**1.78231**	**0.00038**	**0.93387**	**0.00053**	**0.00075**	**3.97458**	**0.00065**	**0.00007**	**0.00003**
	Second Preburn Leach Data (before blank subtraction)								
Mass (g)	3.44E-06	2.67E-08	2.31E-06	1.16E-08	4.36E-06	8.39E-06	6.76E-06	5.74E-09	4.14E-09
Part. equiv.	**0.00491**	**0.00004**	**0.00330**	**0.00002**	**0.00622**	**0.01198**	**0.00966**	**0.00001**	**0.00001**
	Combined Preburn Leach Data (before blank subtraction)								
Mass (g)	1.25E-03	2.93E-07	6.56E-04	3.82E-07	4.88E-06	2.79E-03	7.22E-06		
Part. equiv.	**1.78723**	**0.00042**	**0.93716**	**0.00055**	**0.00697**	**3.98656**	**0.01031**		
	First Postburn Leach Data (before blank subtraction)								
Mass (g)	1.99E-07	1.18E-07	2.93E-08	3.64E-04	6.34E-04	3.82E-07	2.00E-03	1.71E-08	1.64E-08
Part. equiv.	**0.00028**	**0.00017**	**0.00004**	**0.51999**	**0.90580**	**0.00055**	**2.86185**	**0.00002**	**0.00002**
	Second Postburn Leach Data (before blank subtraction)								
Mass (g)	5.45E-09	1.06E-08	2.82E-09	2.36E-04	1.99E-06	1.11E-08	4.46E-04	1.95E-09	3.34E-09
Part. equiv.	**0.00001**	**0.00002**	**0.00000**	**0.33659**	**0.00285**	**0.00002**	**0.63713**	**0.00000**	**0.00000**
	Third Postburn Leach Data (before blank subtraction)								
Mass (g)				3.70E-04			1.37E-04		3.34E-09
Part. equiv.				**0.52869**			**0.19560**		**0.00000**
	Fourth Postburn Leach Data (before blank subtraction)								
Mass (g)				3.47E-06			1.25E-06		3.34E-09
Part. equiv.				**0.00496**			**0.00178**		**0.00000**
	Fifth Postburn Leach Data (before blank subtraction)								
Mass (g)				3.52E-06			2.01E-06		3.34E-09
Part. equiv.				**0.00503**			**0.00288**		**0.00000**
	Combined Postburn Leach Data (before blank subtraction)								
Mass (g)	2.05E-07	1.29E-07	3.21E-08	9.77E-04	6.36E-04	3.93E-07	2.59E-03		
Part. equiv.	**0.00029**	**0.00018**	**0.00005**	**1.39525**	**0.90865**	**0.00056**	**3.69924**		
	Combined Leach-Burn-Leach Data (before blank subtraction)								
Mass (g)	1.25E-03	4.22E-07	6.56E-04	9.77E-04	6.41E-04	2.79E-03	2.60E-03		
Part. equiv.	**1.78752**	**0.00060**	**0.93721**	**1.39580**	**0.91562**	**3.98712**	**3.70955**		

Note: The one-sigma uncertainties in the measured data were estimated to be ~10%, based on multiple ICP-MS measurements of standard samples; however, values are presented with additional significant figures for ease of comparison between leaches.
a. A blank was not processed during postburn leaches 3–5, so the results from postburn leach 2 were used for blank subtraction.

The amounts of uranium detected in the preburn leach phase indicated that ORNL-A, ORNL-C, and ORNL-F contained particles with simulated exposed-kernel defects (Table 4-1). The combined particle equivalents of uranium in the preburn leachates from these three samples were 1.79, 0.94, and 3.99, respectively, and these values rounded to 0.01 were not changed by the blank subtraction (Table 4-2). In

addition, the amounts of uranium in the subsequent postburn ORNL-A, ORNL-C, and ORNL-F leachates did not add any significant fraction of a particle equivalent to the total amounts of uranium measured for each sample. This indicates that there were no particles with simulated SiC defects in these three samples and that near-complete leaching occurred in the preburn leaching of the simulated exposed-kernel defects. As discussed in Section 2.1, the standard practice for QC acceptance testing is to round these values to the nearest whole number (i.e., 2, 1, and 4, respectively) with the assumption that the measured uranium came from discrete particles and then compare the values to a specification for the exposed-kernel defect fraction, which is treated as an attribute property (Marshall 2017; Kercher and Hunn 2005). The exposed-kernel defect populations of one for ORNL-C, two for ORNL-A, and four for ORNL-F match the data provided for these three samples in the round-robin answer key in Appendix A. The deviations from an exact integer value for the particle equivalents of uranium measured for these samples can be explained by variability in uranium loading and the uncertainty in the mass spectrometry analysis for uranium in the leachates. Note that the kernel-to-kernel variation in uranium loading is expected to be much higher than what might be incorrectly inferred from the standard deviation reported by Gerczak et al. (2022) of 0.24%, because that value is a measure of the deviation in the measurement of three particle samples containing several thousand particles each, similar to the uranium-loading analysis reported in Table 3-3.

Table 4-2. Uranium in simulated sample leachates: blank-subtracted values

	Leach-Burn-Leach of Simulated Samples						
	ORNL-A	ORNL-B	ORNL-C	ORNL-D	ORNL-E	ORNL-F	ORNL-G
	First Preburn Leach Data (after blank subtraction)						
Uranium (U) in leachate (g)	1.25E-03	2.19E-07	6.54E-04	3.46E-07	4.99E-07	2.78E-03	4.31E-07
Particle equivalents of U in leachate	**1.78225**	**0.00031**	**0.93380**	**0.00049**	**0.00071**	**3.97454**	**0.00062**
	Second Preburn Leach Data (after blank subtraction)						
Uranium (U) in leachate (g)	3.44E-06	2.09E-08	2.30E-06	7.46E-09	4.35E-06	8.38E-06	6.76E-06
Particle equivalents of U in leachate	**0.00491**	**0.00003**	**0.00329**	**0.00001**	**0.00622**	**0.01197**	**0.00965**
	Combined Preburn Leach Data (after blank subtraction)						
Uranium (U) in leachates (g)	1.25E-03	2.40E-07	6.56E-04	3.54E-07	4.85E-06	2.79E-03	7.19E-06
Particle equivalents of U in leachates	**1.78715**	**0.00034**	**0.93709**	**0.00051**	**0.00693**	**3.98652**	**0.01027**
	First Postburn Leach Data (after blank subtraction)						
Uranium (U) in leachate (g)	1.82E-07	1.01E-07	1.22E-08	3.64E-04	6.34E-04	3.65E-07	2.00E-03
Particle equivalents of U in leachate	**0.00026**	**0.00014**	**0.00002**	**0.51997**	**0.90578**	**0.00052**	**2.86183**
	Second Postburn Leach Data (after blank subtraction)						
Uranium (U) in leachate (g)	3.50E-09	8.61E-09	8.68E-10	2.36E-04	1.99E-06	7.79E-09	4.46E-04
Particle equivalents of U in leachate	**0.00000**	**0.00001**	**0.00000**	**0.33658**	**0.00284**	**0.00001**	**0.63712**
	Third Postburn Leach Data (after blank subtraction)						
Uranium (U) in leachate (g)				3.70E-04			1.37E-04
Particle equivalents of U in leachate				**0.52868**			**0.19560**
	Fourth Postburn Leach Data (after blank subtraction)						
Uranium (U) in leachate (g)				3.47E-06			1.24E-06
Particle equivalents of U in leachate				**0.00496**			**0.00178**
	Fifth Postburn Leach Data (after blank subtraction)						
Uranium (U) in leachate (g)				3.52E-06			2.01E-06
Particle equivalents of U in leachate				**0.00502**			**0.00287**
	Combined Postburn Leach Data (after blank subtraction)						
Uranium (U) in leachates (g)	1.86E-07	1.10E-07	1.31E-08	9.77E-04	6.36E-04	3.73E-07	2.59E-03
Particle equivalents of U in leachates	**0.00027**	**0.00016**	**0.00002**	**1.39521**	**0.90862**	**0.00053**	**3.69919**
	Combined Leach-Burn-Leach Data (after blank subtraction)						
Uranium (U) in leachates (g)	1.25E-03	3.50E-07	6.56E-04	9.77E-04	6.41E-04	2.79E-03	2.60E-03
Particle equivalents of U in leachates	**1.78742**	**0.00050**	**0.93710**	**1.39572**	**0.91555**	**3.98705**	**3.70946**

Note: See footnotes in Table 4-1.

The amounts of uranium in the ORNL-D, ORNL-E, and ORNL-G leaches indicated the presence of simulated SiC defects. However, the data were complicated by premature leaching before the burn and

incomplete leaching after the burn. The particle equivalents of uranium measured in the ORNL-D, ORNL-E, and ORNL-G preburn leachates were 0.00055, 0.0070, and 0.010, respectively (Table 4-1). These low values indicate the absence of simulated exposed-kernel defects. However, comparing all four samples with no simulated exposed-kernel defects reveals that the uranium values for ORNL-E and ORNL-G were significantly higher than ORNL-B and ORNL-D. In addition, the second ORNL-E and ORNL-G preburn leachates, although relatively low from a particle defect perspective at <0.01 particle equivalents, had more uranium than the corresponding first preburn leachates. This suggests that acid was slowly infiltrating the exposed IPyC layers in the particles with simulated SiC defects contained in ORNL-E and ORNL-G. Similar behavior was observed and studied during the development work for fabricating the postburn leach defect particles (Gerczak et al. 2022). During those development efforts, ten particles, each having one 25 µm diameter FIB-milled hole through the SiC to simulate a local SiC defect (Figure 1-2), were subjected to LBL in two sets of five to verify the performance of the defects. Approximately 4–5% of the total uranium inventory in each five-particle set was measured in the preburn leach phase, and most of this was detected in the second 24 h leachate (the same behavior as that observed in ORNL-E and ORNL-G). X-ray computed tomography performed on the particles after preburn leaching and before the burn showed uranium dispersed in the buffer layer (Figure 4-1a), suggesting that the nitric acid had slowly penetrated the intact but exposed IPyC layer during the preburn leaches and uranium was being leached out of the kernel. After postburn leaching of the two sets of five particles with simulated SiC defects, combined LBL totals of 4.8 and 4.9 particle equivalents of uranium were measured in the leachates. After this postburn leaching, recovered particles were again subjected to XCT, which showed empty SiC shells (Figure 4-1b) with no significant residual uranium remaining from the leached kernels (Gerczak et al. 2022).

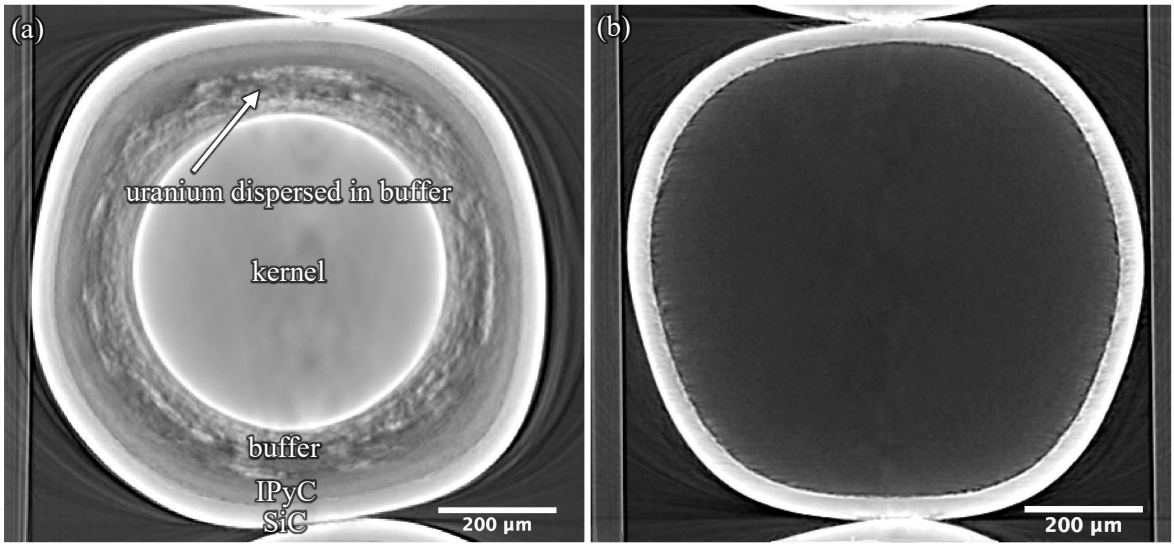

Figure 4-1. XCT tomograms of a particle with a simulated SiC defect. (a) Particle after preburn leaching showing uranium dispersion in the buffer, and (b) same particle after postburn leaching, in which buffer and IPyC were oxidized and removed during the burn phase and kernel material was removed during the postburn leach phase. Images from Gerczak et al. (2022).

The total particle equivalents of uranium measured in the ORNL-D, ORNL-E, and ORNL-G leachates were 1.4, 0.92, and 3.7 (Table 4-1), with almost all of this in the postburn leachates, which indicated the presence of particles with simulated SiC defects. The total measured values were all lower than the expected integral values (Appendix Table A-1). However, the deviations from integral values for ORNL-E and ORNL-G were within a range that could be explained by kernel-to-kernel variation and the estimated 10% ICP-MS uncertainty. The measured values for these two samples rounded to one simulated SiC defect in ORNL-E and four simulated SiC defects in ORNL-G, in agreement with the answer key. In contrast, the uranium in the ORNL-D leachates was notably 0.6 particle equivalents less than the expected

average uranium in two particles. Based on a postburn leach result of 1.4 particle equivalents of uranium, the total number of particles with SiC defects in ORNL-D would be identified as "one" according to the guidelines in some HTGR reactor fuel specifications, which would underrepresent the number of particles with simulated SiC defects known to be in this round-robin sample. However, as discussed in Section 2.1, deviations beyond the expected, especially in conjunction with unusual leaching behavior as observed in ORNL-D should be considered suspect and further investigated.

Figure 4-2 is a stacked plot that graphically displays the blank-subtracted particle equivalents of uranium reported in Table 4-2 for each successive leachate. The samples seeded with simulated exposed-kernel defects (ORNL-A, ORNL-C, and ORNL-F) and the sample seeded with a single SiC defect (ORNL-E) showed ideal, near-complete leaching during the first 24 h leach before or after the burn, as appropriate for the type of defect. The second postburn leachate from ORNL-E showed a 99.7% decrease in uranium content compared with the first postburn leachate, providing confidence that leaching was sufficiently complete. In contrast, postburn leach results were atypical for ORNL-D and ORNL-G. Both samples had unusually high second 24 h postburn leaches compared with the corresponding first 24 h preburn leaches. As discussed above, this warranted follow-on leaching. To save time iterating between leaching and leachate analysis, three additional postburn leaches were performed on both samples. In both cases, the fourth leach was low enough to consider further leaching unnecessary, and the fifth leach simply provided further confidence that negligible accessible uranium remained. The results from additional leaching of ORNL-D and ORNL-G are good examples of the importance of analyzing successive leaches to confirm sufficient leaching for enumeration of defective particles and conducting additional leaches until the uranium content in the last leachate in a series is below the MDL or less than a significant fraction of the uranium previously measured during that leaching phase.

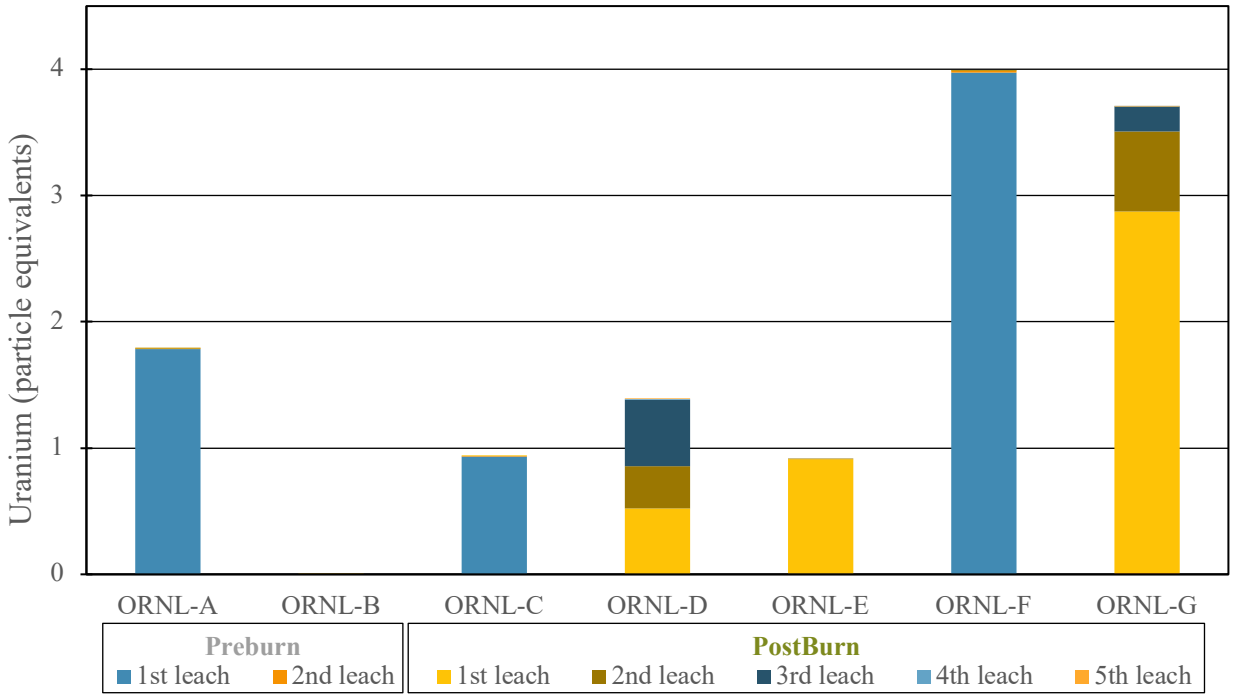

Figure 4-2. Fraction of uranium single particle equivalent content in each leach.

The postburn leach results shown in Table 4-2 and Figure 4-2 suggest slow-leaching of at least two kernels in ORNL-D and at least one kernel in ORNL-G. Leaching beyond the fourth leach did not appear to be warranted, as the fourth leach added a negligible fraction to the total and confirmed leaching was sufficient. The additional third and fourth postburn leaches of ORNL-G were successful in measuring enough uranium to identify the presence of four simulated SiC defects. However, the ORNL-D results

were still considered suspect after the additional postburn leaches were analyzed because the total particle equivalents of uranium were outside of the expected deviation from an integral value. When atypical results are observed in an LBL analysis, additional exploratory analysis can often be employed to further explore the presence and behavior of defective particles. Two methods successfully employed at ORNL after LBL to identify and isolate defective particles for microstructural analysis are (1) to selectively float hollow particles in an appropriate density liquid and (2) to subject the particles to x-ray radiography. After LBL, ORNL-D particles were placed in a bromoform solution, and acetone was systematically added in an attempt to reach a density that would be less than the density of the coated ZrO_2 particles but greater than the density of the leached particles, so that the leached particles would float while the others sank. This was unsuccessful, probably due to liquid inside the leached particles, as discussed below. Therefore, all the ORNL-D particles were sandwiched in a single layer between Kapton tape, and low-resolution x-ray radiographs were obtained. Figure 4-3 shows two abnormal particles that were identified in the radiographs. These two particles were labeled ORNL-D-1 and ORNL-D-2 and extracted from the Kapton tape for further analysis.

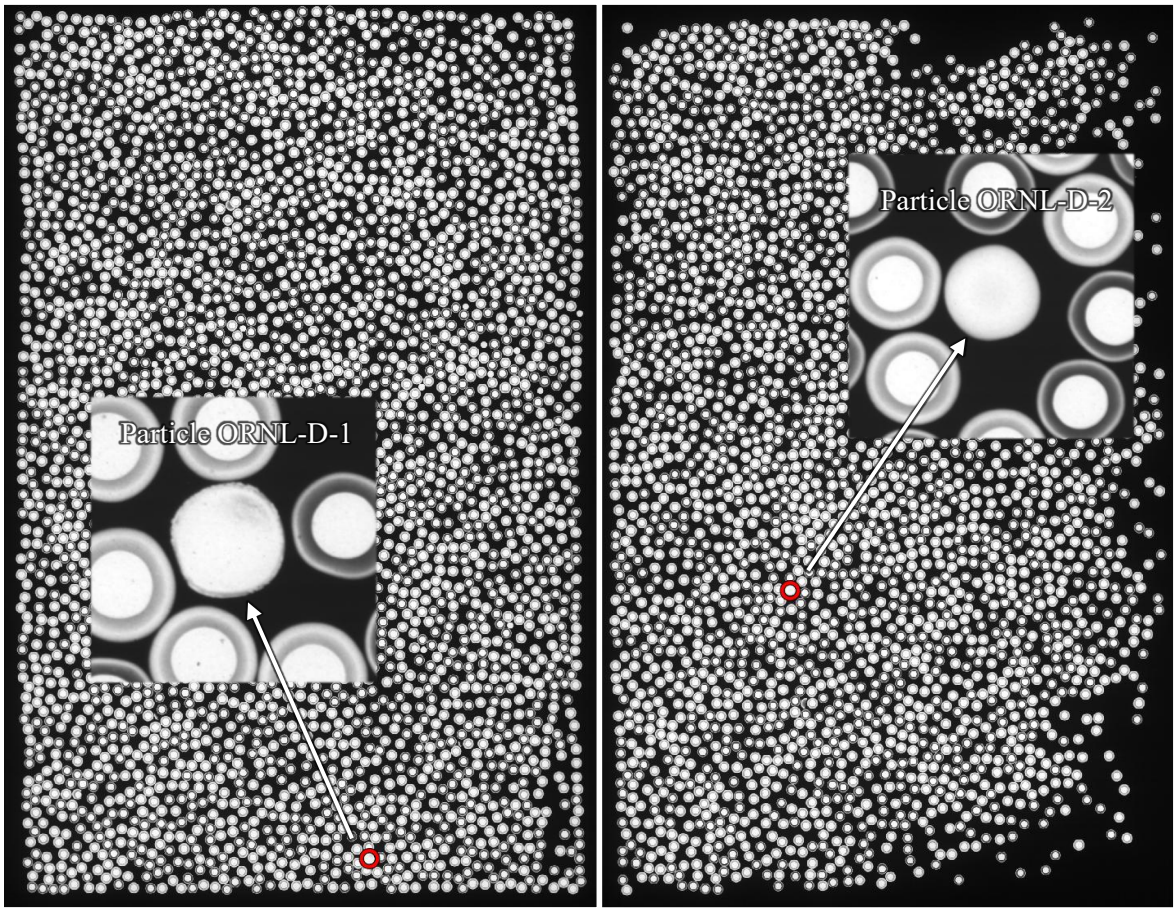

Figure 4-3. X-ray radiography identified two particles with simulated SiC defects (ORNL-D-1 and ORNL-D-2) hidden among the coated ZrO_2 particles. Note: the variable appearance of the coated ZrO_2 particles is due to two batches with different SiC thickness being blended to provide enough particles to make all 21 simulated samples for the LBL round-robin test.

The two abnormal particles isolated from ORNL-D were subjected to XCT, and tomograms of a select cross section through each particle are shown in Figure 4-4. Examination of the three-dimensional data from the XCT reconstruction revealed the presence of a FIB-milled hole in each particle, which confirmed that these were the two particles with simulated SiC defects that had been added to ORNL-D, (see Appendix Table A-1). Both particles had liquid trapped inside the SiC shell, as indicated by an

elevated x-ray density in the interior volume except where an air bubble had formed. It is not known whether this liquid was bromoform from the attempt to separate the particles using a sink-float technique or residual acid from the leaching. Figure 4-4a shows bright regions inside the SiC shell of Particle ORNL-D-1 that indicate the presence of material of significantly higher density than the SiC or surrounding liquid medium. This was presumably unleached U_3O_8 formed during the burn phase when the kernel was oxidized. This material was distributed in the liquid inside of the SiC shell and had apparently settled in the lower half due to gravity (the vertical orientations shown in Figure 4-4 are the same as the orientations of the particles in the holder during x-ray imaging). No residual kernel material was visible in the XCT images of Particle ORNL-D-2 (Figure 4-4b), which indicates that this particle was sufficiently leached by the supplemental postburn leaches. However, the supplemental leaches were not successful in leaching all the uranium from Particle ORNL-D-1, perhaps due to plugging of the FIB-milled hole, and this explains the deviation from the expected value of approximately 2 particle equivalents for the total uranium measured in the ORNL-D leachates.

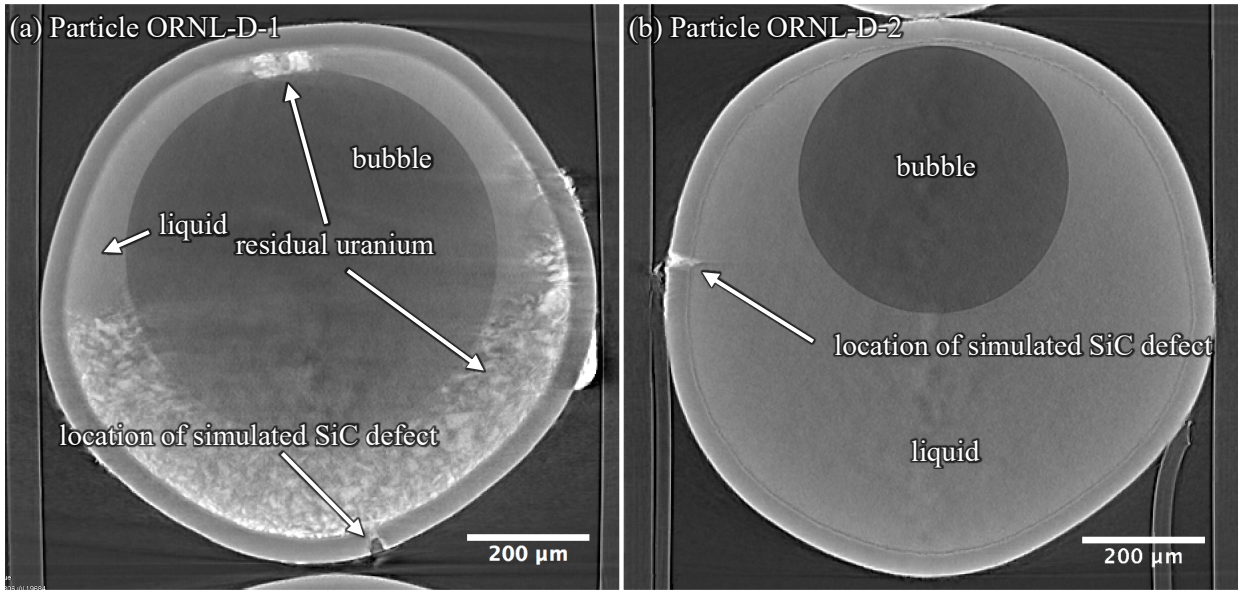

Figure 4-4. XCT tomograms of the two particles with confirmed simulated SiC defects recovered from the ORNL-D simulated sample after postburn leaching was complete. (a) Particle ORNL-D-1 showing location of FIB-milled hole and residual uranium present inside SiC and (b) Particle ORNL-D-2 showing location of FIB-milled hole and only liquid inside the SiC.

4.2 IMPURITY ANALYSIS BY LEACH-BURN-LEACH

Measured data for the nonuranium elements contained in the NIST SRM 1632d coal impurity standard that were targeted for analysis are presented in Table 4-3 and Table 4-4 for the first and second preburn leaches and first and second postburn leaches, respectively. Measurable quantities of all the impurity elements of interest were detected in the first preburn leachate, and, in most cases, what was measured in the first preburn leachate represented the greater part of the total measured amount, as discussed in more detail below. For the representative sublots discussed in Section 3.3, many of the impurity elements were present in very low concentrations that were sometimes of the same order of magnitude as what was measured in the high-purity acid blanks. In contrast, for the simulated samples, blank values were generally negligible fractions of the first preburn leach values. Most elements had first preburn leach blank-to-sample ratios of <1%, with the exception of Ca, Cr, Ni, and Eu, which ranged from 1%–7%, and Sb, which had a ratio of ~10%. This result indicates that contamination introduced during analysis had negligible or only minor effects on the cumulative impurity content measured in the simulated samples. Blank subtraction was not applied to the impurity data presented in this section for the sake of simplicity

and conciseness in the discussion of the results, as well as because blank subtraction provides only a rough estimate of the possible background contamination in each sample. Forgoing blank subtraction is consistent with the approach used at ORNL for QC acceptance testing, in which data from the analysis of acid blanks is used to monitor for unusually high background contamination that would indicate a problem with the analysis process, but the blank values are not subtracted from the sample results when comparing measured LBL data with the specified impurity limits. This comparison provides a conservative test for acceptance because samples affected by background contamination might be falsely rejected, but falsely accepting a sample with excessive impurity content after subtracting an overestimation of the contribution from background correction is avoided.

Table 4-3. Impurities in simulated sample preburn leachates: measured values

Impurity in leachate	Preburn Leach of Simulated Samples							BLANK	BLANK
	ORNL-A	ORNL-B	ORNL-C	ORNL-D	ORNL-E	ORNL-F	ORNL-G		
	First Preburn Leach Data (before blank subtraction)								
Al (g)	2.00E-03	1.74E-03	1.71E-03	1.51E-03	1.34E-03	1.54E-03	1.47E-03	1.14E-05	4.64E-06
Ca (g)	6.97E-04	6.54E-04	6.49E-04	6.64E-04	6.64E-04	6.53E-04	5.87E-04	1.24E-05	6.10E-06
Ti (g)	1.83E-04	1.40E-04	1.46E-04	1.42E-04	1.39E-04	1.43E-04	1.35E-04	6.05E-07	6.55E-08
V (g)	1.09E-05	1.02E-05	1.05E-05	1.00E-05	9.87E-06	1.01E-05	9.01E-06	< 7.5E-09	< 7.2E-09
Cr (g)	6.55E-06	6.15E-06	7.10E-06	6.31E-06	6.23E-06	6.13E-06	5.82E-06	4.16E-07	9.37E-08
Mn (g)	6.68E-06	6.15E-06	6.62E-06	6.18E-06	6.05E-06	6.05E-06	5.53E-06	< 2.5E-08	< 2.4E-08
Fe (g)	5.08E-03	3.85E-03	3.81E-03	3.44E-03	3.51E-03	3.59E-03	3.35E-03	1.35E-05	< 2.7E-06
Co (g)	1.89E-06	1.73E-06	1.82E-06	1.74E-06	1.69E-06	1.74E-06	1.52E-06	1.00E-08	< 2.7E-09
Ni (g)	5.42E-06	4.99E-06	6.06E-06	5.10E-06	5.05E-06	5.18E-06	4.42E-06	2.73E-07	1.10E-07
Sb (g)	2.89E-08	1.79E-08	2.58E-08	3.93E-08	3.20E-08	3.13E-08	2.98E-08	3.00E-09	2.73E-09
Ba (g)	1.76E-05	1.55E-05	1.63E-05	1.44E-05	1.51E-05	1.52E-05	1.39E-05	1.00E-07	2.78E-08
Cd (g)	3.75E-08	3.78E-08	3.42E-08	4.57E-08	4.03E-08	3.70E-08	4.17E-08	< 7.1E-09	< 6.8E-09
Ce (g)	5.25E-06	4.60E-06	4.90E-06	4.98E-06	5.05E-06	5.13E-06	4.76E-06	2.73E-08	5.46E-10
Cs (g)	2.78E-07	2.51E-07	2.65E-07	2.49E-07	2.50E-07	2.64E-07	2.20E-07	5.68E-10	< 8.3E-11
Eu (g)	1.34E-07	1.16E-07	1.20E-07	1.09E-07	1.07E-07	1.12E-07	1.01E-07	5.58E-09	3.64E-10
Rb (g)	2.65E-06	2.49E-06	2.64E-06	2.23E-06	2.19E-06	2.33E-06	1.87E-06	< 1.8E-09	< 1.7E-09
Sr (g)	3.57E-05	3.17E-05	3.35E-05	3.00E-05	2.99E-05	3.11E-05	2.78E-05	2.14E-08	< 1.4E-08
Th (g)	6.55E-07	5.55E-07	6.15E-07	6.43E-07	6.83E-07	7.00E-07	6.50E-07	1.80E-09	9.10E-11
	Second Preburn Leach Data (before blank subtraction)								
Al (g)	1.59E-03	1.42E-03	1.54E-03	1.29E-03	8.90E-04	1.30E-03	1.19E-03	3.41E-06	1.73E-06
Ca (g)	1.33E-05	1.31E-05	1.02E-05	1.88E-05	1.98E-05	2.07E-05	2.00E-05	7.04E-06	1.53E-05
Ti (g)	2.54E-05	2.15E-05	2.44E-05	2.51E-05	1.98E-05	2.91E-05	2.82E-05	4.82E-07	8.14E-08
V (g)	1.07E-06	8.93E-07	9.67E-07	8.99E-07	6.61E-07	8.40E-07	8.65E-07	< 7.3E-09	< 7.0E-09
Cr (g)	8.22E-07	6.84E-07	7.55E-07	6.89E-07	5.30E-07	6.66E-07	6.72E-07	9.72E-08	2.71E-08
Mn (g)	2.79E-07	2.34E-07	2.34E-07	3.39E-07	1.98E-07	2.56E-07	2.62E-07	< 2.4E-08	< 2.3E-08
Fe (g)	7.83E-05	6.55E-05	6.85E-05	7.77E-05	6.19E-05	7.78E-05	7.35E-05	4.82E-06	5.63E-06
Co (g)	2.05E-08	2.05E-08	1.68E-08	1.48E-08	1.08E-08	1.47E-08	1.39E-08	3.06E-09	2.82E-09
Ni (g)	3.95E-07	1.93E-07	3.23E-07	< 4.3E-08	< 4.3E-08	< 4.6E-08	2.91E-07	9.63E-08	< 4.5E-08
Sb (g)	6.44E-09	4.85E-09	2.57E-09	1.21E-08	7.21E-09	9.30E-09	1.39E-08	< 1.5E-09	< 1.4E-09
Ba (g)	3.17E-06	2.88E-06	2.97E-06	2.60E-06	1.82E-06	2.52E-06	2.52E-06	< 9.1E-09	< 8.6E-09
Cd (g)	< 6.5E-09	< 6.4E-09	< 6.2E-09	< 6.3E-09	< 6.4E-09	< 6.7E-09	< 6.7E-09	< 6.9E-09	< 6.6E-09
Ce (g)	5.57E-07	4.59E-07	5.02E-07	4.33E-07	3.72E-07	4.43E-07	3.90E-07	5.09E-09	3.52E-10
Cs (g)	5.18E-08	4.29E-08	4.48E-08	5.17E-08	3.63E-08	4.47E-08	5.78E-08	9.26E-11	< 8.0E-11
Eu (g)	6.09E-09	5.70E-09	5.64E-09	4.87E-09	3.99E-09	4.65E-09	4.30E-09	< 1.0E-10	1.76E-10
Rb (g)	1.02E-06	8.80E-07	9.01E-07	9.32E-07	6.53E-07	8.58E-07	1.00E-06	< 1.7E-09	< 1.7E-09
Sr (g)	1.02E-06	9.01E-07	9.21E-07	8.40E-07	7.21E-07	8.54E-07	7.35E-07	< 1.4E-08	< 1.3E-08
Th (g)	3.83E-08	2.91E-08	3.42E-08	2.69E-08	2.35E-08	2.79E-08	2.62E-08	1.85E-10	< 6.5E-11

Note: Less-than values (displayed in gray) indicate the concentration in the aliquot was below the MDL.
Note: The nine QC-relevant impurities reported for the representative sublots in Section 3.3 are listed above the double line.
Note: The one-sigma uncertainties in the measurable data from the first and second leaches were estimated to be ~10%, based on multiple ICP-MS measurements of standard samples. However, values are presented with additional significant figures, in some cases, for ease of comparison between leaches.

Table 4-4. Impurities in simulated sample postburn leachates: measured values

Impurity in leachate	Postburn Leach of Simulated Samples							BLANK	BLANK
	ORNL-A	ORNL-B	ORNL-C	ORNL-D	ORNL-E	ORNL-F	ORNL-G		
	First Postburn Leach Data (before blank subtraction)								
Al (g)	1.46E-03	1.12E-03	1.30E-03	1.44E-03	1.84E-03	1.39E-03	1.15E-03	5.96E-06	3.79E-06
Ca (g)	6.15E-06	1.08E-05	6.76E-06	< 5.7E-06	8.45E-06	1.06E-05	< 5.6E-06	< 6.1E-06	< 5.8E-06
Ti (g)	8.22E-06	3.71E-06	5.96E-06	7.16E-06	8.27E-06	5.92E-06	8.53E-06	5.17E-08	< 4.5E-08
V (g)	6.02E-07	3.61E-07	4.05E-07	6.36E-07	7.32E-07	4.90E-07	5.15E-07	2.00E-08	< 7.0E-09
Cr (g)	5.12E-07	3.96E-07	4.45E-07	5.13E-07	5.92E-07	5.12E-07	4.72E-07	8.16E-08	4.40E-08
Mn (g)	2.67E-07	2.03E-07	2.35E-07	2.04E-07	2.62E-07	2.06E-07	2.38E-07	3.64E-08	< 2.3E-08
Fe (g)	3.48E-05	2.73E-05	3.07E-05	3.59E-05	4.57E-05	3.69E-05	3.39E-05	2.98E-06	< 2.6E-06
Co (g)	2.54E-08	2.56E-08	2.25E-08	1.07E-07	1.78E-08	1.83E-08	1.89E-08	< 2.8E-09	< 2.7E-09
Ni (g)	2.32E-06	2.56E-06	2.84E-06	2.60E-06	2.02E-06	2.37E-06	2.04E-06	4.60E-07	1.28E-07
Sb (g)	8.71E-09	5.53E-09	6.32E-09	1.16E-08	7.14E-09	7.48E-09	1.33E-08	3.26E-09	3.03E-09
Ba (g)	2.87E-06	2.10E-06	2.64E-06	2.76E-06	3.24E-06	2.75E-06	2.56E-06	2.71E-08	5.56E-08
Cd (g)	< 6.7E-09	1.20E-08	< 6.7E-09	< 6.6E-09	< 6.8E-09	< 6.7E-09	< 6.5E-09	< 7.0E-09	< 6.7E-09
Ce (g)	2.08E-07	1.59E-07	1.84E-07	2.21E-07	3.10E-07	2.18E-07	1.54E-07	4.29E-09	9.79E-10
Cs (g)	2.21E-08	1.74E-08	1.93E-08	2.28E-08	2.98E-08	2.23E-08	2.06E-08	9.32E-11	1.78E-10
Eu (g)	2.33E-09	2.53E-09	2.23E-09	3.80E-09	2.71E-09	2.67E-09	6.24E-09	7.46E-10	8.90E-10
Rb (g)	6.06E-07	4.40E-07	5.38E-07	6.14E-07	7.59E-07	5.96E-07	5.46E-07	< 1.8E-09	< 1.7E-09
Sr (g)	4.49E-07	3.38E-07	4.16E-07	4.38E-07	5.51E-07	4.37E-07	3.62E-07	< 1.4E-08	< 1.3E-08
Th (g)	8.62E-09	7.69E-09	8.72E-09	1.06E-08	1.37E-08	1.12E-08	9.79E-09	1.86E-10	8.90E-11
	Second Postburn Leach Data (before blank subtraction)								
Al (g)	3.32E-05	3.09E-05	1.82E-05	3.22E-05	6.57E-05	2.85E-05	2.03E-05	3.28E-06	2.79E-06
Ca (g)	< 5.8E-06	< 6.2E-06	< 5.9E-06	< 5.8E-06	< 5.9E-06	< 5.7E-06	< 6.1E-06	< 6.0E-06	< 5.4E-06
Ti (g)	2.25E-06	1.29E-06	3.31E-06	3.26E-06	3.29E-06	3.22E-06	4.15E-06	< 4.7E-08	1.24E-07
V (g)	3.86E-08	8.21E-08	1.02E-07	3.36E-08	6.93E-08	6.96E-08	1.03E-08	< 7.3E-09	< 6.6E-09
Cr (g)	7.60E-08	6.48E-08	7.33E-08	8.94E-08	9.38E-08	6.31E-08	7.63E-08	3.75E-08	3.24E-08
Mn (g)	< 2.3E-08	< 2.5E-08	< 2.4E-08	< 2.3E-08	< 2.3E-08	< 2.3E-08	< 2.4E-08	< 2.4E-08	< 2.2E-08
Fe (g)	3.42E-06	3.72E-06	3.59E-06	8.32E-06	5.35E-06	3.81E-06	< 2.8E-06	< 2.8E-06	< 2.5E-06
Co (g)	4.02E-09	< 2.9E-09	< 2.7E-09	5.43E-09	< 2.7E-09	< 2.6E-09	< 2.8E-09	< 2.8E-09	5.92E-09
Ni (g)	< 4.6E-08	< 4.9E-08	5.51E-08	< 4.5E-08	< 4.6E-08	< 4.5E-08	< 4.8E-08	< 4.7E-08	< 4.3E-08
Sb (g)	6.35E-09	3.17E-09	3.64E-09	6.76E-09	4.35E-09	3.07E-09	9.08E-09	< 1.5E-09	< 1.3E-09
Ba (g)	1.73E-07	1.76E-07	7.96E-08	1.21E-07	2.99E-07	1.05E-07	5.52E-08	< 9.1E-09	1.29E-08
Cd (g)	< 6.7E-09	< 7.2E-09	< 6.8E-09	< 6.7E-09	< 6.8E-09	< 6.6E-09	< 7.0E-09	< 7.0E-09	< 6.3E-09
Ce (g)	1.34E-09	1.92E-09	2.09E-09	2.94E-09	2.36E-09	2.80E-09	3.74E-09	2.14E-09	5.84E-10
Cs (g)	1.16E-09	1.15E-09	4.55E-10	6.23E-10	1.63E-09	5.26E-10	9.36E-11	9.30E-11	8.34E-11
Eu (g)	2.68E-10	1.92E-10	2.73E-10	1.78E-10	< 9.8E-11	< 9.5E-11	1.87E-10	2.79E-10	< 9.0E-11
Rb (g)	2.54E-08	2.66E-08	1.15E-08	1.56E-08	4.38E-08	1.10E-08	5.05E-09	< 1.8E-09	< 1.6E-09
Sr (g)	2.54E-08	2.19E-08	1.66E-08	1.93E-08	3.67E-08	1.77E-08	< 1.4E-08	< 1.4E-08	< 1.2E-08
Th (g)	8.05E-10	6.72E-10	7.28E-10	1.69E-09	1.45E-09	1.66E-09	1.97E-09	9.30E-11	< 6.1E-11

Note: See footnotes in Table 4-3.

Table 4-5 and Table 4-6 show the measured impurity data from the third, fourth, and fifth leaches of ORNL-D and ORNL-G, respectively. The combined LBL data with and without the inclusion of these leaches are also shown. The combined data are presented as single values or as a range in the same manner described for Table 3-4 in Section 3.3, with the ranges representing minimum and maximum possible values based on the assumption that measurements below the MDL could have been as low as zero and as high as the MDL. As indicated by the percent change to the cumulative results shown in the rightmost column of Table 4-5 and Table 4-6, the contribution from postburn leachates 3–5 to the total measured amount of each impurity was negligible in most cases. Some elements showed a broader range between the possible minimum and maximum values due to multiple leachates having content below the MDL for that element. Cadmium was an extreme example because it was only present in a measurable concentration in the first preburn leachate and the MDLs were a significant fraction (14%–18%) of what was measured in the first leachate. As such, summation of successive leachates below the MDL with the

assumption that the value was as high as the MDL significantly elevated the perceived content. This result demonstrates an inherent issue with interpreting LBL results because the number of leachates performed can artificially affect the result if the MDL is assumed as a conservative estimate on the upper bound of the impurity content in each leachate (i.e., the more leaches performed, the higher the acceptance test value becomes). This effect should be considered when summing data for an element with consecutive measurements below the MDL.

Table 4-5. Impurities in additional ORNL-D postburn leachates: measured values

Impurity in leachate	Additional Postburn Leaches of Simulated Sample ORNL-D (before blank subtraction)					
	Preburn + Postburn 1–2	Leachate 3	Leachate 4	Leachate 5	Preburn + Postburn 1–5	Percent Change
Al (g)	4.27E-03	5.53E-06	3.76E-06	4.07E-06	4.29E-03	0.3%
Ca (g)	6.83E-04 – 6.94E-04	< 6.1E-06	< 6.1E-06	< 6.2E-06	6.83E-04 – 7.13E-04	0.0% – 2.7%
Ti (g)	1.77E-04	8.23E-07	1.04E-06	1.46E-06	1.80E-04	1.9%
V (g)	1.16E-05	< 7.5E-09	< 7.5E-09	< 7.6E-09	1.16E-05 – 1.16E-05	0.0% – 0.2%
Cr (g)	7.60E-06	8.66E-08	6.47E-08	8.29E-08	7.83E-06	3.1%
Mn (g)	6.73E-06 – 6.75E-06	< 2.5E-08	< 2.4E-08	< 2.5E-08	6.73E-06 – 6.82E-06	0.0% – 1.1%
Fe (g)	3.56E-03	4.48E-06	3.96E-06	3.41E-06	3.57E-03	0.3%
Co (g)	1.87E-06	7.66E-09	1.81E-08	2.98E-08	1.92E-06	3.0%
Ni (g)	7.70E-06 – 7.79E-06	1.13E-06	< 4.8E-08	< 4.9E-08	8.83E-06 – 9.01E-06	14.6% – 15.7%
Sb (g)	6.98E-08	< 1.5E-09	< 1.5E-09	< 1.5E-09	6.98E-08 – 7.44E-08	0.0% – 6.6%
Ba (g)	1.98E-05	4.92E-08	1.13E-08	< 9.4E-09	1.99E-05 – 1.99E-05	0.3% – 0.4%
Cd (g)	4.57E-08 – 6.53E-08	< 7.1E-09	< 7.1E-09	< 7.2E-09	4.57E-08 – 8.66E-08	0.0% – 32.7%
Ce (g)	5.64E-06	1.51E-09	1.23E-09	7.66E-10	5.64E-06	0.1%
Cs (g)	3.24E-07	3.78E-10	2.83E-10	9.58E-11	3.24E-07	0.2%
Eu (g)	1.18E-07	6.62E-10	1.89E-10	1.92E-10	1.19E-07	0.9%
Rb (g)	3.79E-06	2.46E-09	< 1.8E-09	< 1.8E-09	3.79E-06 – 3.80E-06	0.1% – 0.2%
Sr (g)	3.13E-05	1.46E-08	< 1.4E-08	< 1.4E-08	3.13E-05 – 3.13E-05	0.0% – 0.1%
Th (g)	6.82E-07	4.73E-10	5.66E-10	2.87E-10	6.84E-07	0.2%

Note: See footnotes in Table 4-3.
Note: Presented ranges incorporate the MDL as described in the text.

Table 4-6. Impurities in additional ORNL-G postburn leachates: measured values

Impurity in leachate	Additional Postburn Leaches of Simulated Sample ORNL-G (before blank subtraction)					
	Preburn + Postburn 1–2	Leachate 3	Leachate 4	Leachate 5	Preburn + Postburn 1–5	Percent Change
Al (g)	3.83E-03	2.78E-06	4.73E-06	2.86E-06	3.84E-03	0.3%
Ca (g)	6.07E-04 – 6.18E-04	< 5.8E-06	< 5.9E-06	< 6.1E-06	6.07E-04 – 6.36E-04	0.0% – 2.9%
Ti (g)	1.76E-04	7.82E-07	1.29E-06	8.14E-07	1.78E-04	1.6%
V (g)	1.04E-05	< 7.1E-09	< 7.2E-09	< 7.5E-09	1.04E-05 – 1.04E-05	0.0% – 0.2%
Cr (g)	7.04E-06	9.61E-08	6.14E-08	5.58E-08	7.26E-06	3.0%
Mn (g)	6.02E-06 – 6.05E-06	< 2.3E-08	< 2.4E-08	< 2.5E-08	6.02E-06 – 6.12E-06	0.0% – 1.2%
Fe (g)	3.46E-03 – 3.46E-03	5.72E-06	4.22E-06	3.93E-06	3.47E-03 – 3.47E-03	0.4% – 0.4%
Co (g)	1.55E-06 – 1.56E-06	9.12E-09	< 2.7E-09	< 2.9E-09	1.56E-06 – 1.57E-06	0.6% – 0.9%
Ni (g)	6.75E-06 – 6.79E-06	1.19E-07	< 4.6E-08	< 4.8E-08	6.87E-06 – 7.01E-06	1.8% – 3.1%
Sb (g)	6.61E-08	< 1.4E-09	< 1.5E-09	< 1.5E-09	6.61E-08 – 7.05E-08	0.0% – 6.7%
Ba (g)	1.91E-05	1.42E-08	1.58E-08	< 9.3E-09	1.91E-05 – 1.91E-05	0.2% – 0.2%
Cd (g)	4.17E-08 – 6.20E-08	< 6.7E-09	< 6.8E-09	< 7.1E-09	4.17E-08 – 8.26E-08	0.0% – 33.3%
Ce (g)	5.31E-06	1.61E-09	1.91E-09	9.46E-10	5.31E-06	0.1%
Cs (g)	2.99E-07	3.58E-10	1.82E-10	9.46E-11	2.99E-07	0.2%
Eu (g)	1.12E-07	1.79E-10	< 9.9E-11	< 1.0E-10	1.12E-07 – 1.12E-07	0.2% – 0.3%
Rb (g)	3.42E-06	< 1.7E-09	< 1.7E-09	< 1.8E-09	3.42E-06 – 3.43E-06	0.0% – 0.2%
Sr (g)	2.89E-05 – 2.89E-05	< 1.3E-08	< 1.4E-08	< 1.4E-08	2.89E-05 – 2.89E-05	0.0% – 0.1%
Th (g)	6.88E-07	7.15E-10	8.19E-10	3.78E-10	6.90E-07	0.3%

Note: See footnotes in Table 4-5.

The summed values from Table 4-3 and Table 4-4 are provided in Table 4-7. For consistency in comparing the impurity analyses across the seven simulated samples, the data from the third, fourth, and fifth postburn leaches of ORNL-D and ORNL-G were not included in the combined totals in Table 4-7. As shown in Table 4-5 and Table 4-6 and discussed above, the contributions from these extra leaches to the total measured impurity content were negligible for most elements. As was done for Table 3-4 and Table 3-5, possible ranges were calculated for the combined data in Table 4-7, in which the lower value was the sum with each less-than value assumed to be equal to zero (i.e., its minimum possible value), and the upper value was the sum with each less-than value assumed to be equal to the MDL (i.e., its maximum possible value). Only five elements had calculated minimum and maximum summed values that differed in the first three nonzero digits. Four of these elements (Ca, Mn, Ni, and Cd) are presented in Table 4-7 in two rows showing the minimum and maximum summed values. The fifth element (Co) is not presented in the table as two values because the minimum and maximum values differed in only two samples and the differences in those two samples were neglible (~1E-8 g, which was <1% of the total).

Table 4-7. Total impurities measured in two preburn and two postburn leachates for each simulated sample

	Leach-Burn-Leach Analysis of Simulated Samples						
	ORNL-A	ORNL-B	ORNL-C	ORNL-D	ORNL-E	ORNL-F	ORNL-G
	Combined Leach-Burn-Leach Data (before blank subtraction)						
Aluminum (Al) in leachates (g)	5.08E-03	4.31E-03	4.56E-03	4.27E-03	4.13E-03	4.25E-03	3.83E-03
Calcium (Ca) in leachates (g) min.	7.17E-04	6.78E-04	6.66E-04	6.83E-04	6.93E-04	6.84E-04	6.07E-04
Calcium (Ca) in leachates (g) max.	7.22E-04	6.84E-04	6.72E-04	6.94E-04	6.98E-04	6.90E-04	6.18E-04
Titanium (Ti) in leachates (g)	2.19E-04	1.67E-04	1.79E-04	1.77E-04	1.70E-04	1.81E-04	1.76E-04
Vanadium (V) in leachates (g)	1.26E-05	1.16E-05	1.20E-05	1.16E-05	1.13E-05	1.15E-05	1.04E-05
Chromium (Cr) in leachates (g)	7.96E-06	7.29E-06	8.37E-06	7.60E-06	7.45E-06	7.37E-06	7.04E-06
Manganese (Mn) in leachates (g) min.	7.22E-06	6.59E-06	7.09E-06	6.73E-06	6.51E-06	6.51E-06	6.02E-06
Manganese (Mn) in leachates (g) max.	7.25E-06	6.61E-06	7.11E-06	6.75E-06	6.54E-06	6.53E-06	6.05E-06
Iron (Fe) in leachates (g)	5.20E-03	3.95E-03	3.92E-03	3.56E-03	3.63E-03	3.71E-03	3.46E-03
Cobalt (Co) in leachates (g)	1.94E-06	1.77E-06	1.86E-06	1.87E-06	1.72E-06	1.77E-06	1.55E-06
Nickel (Ni) in leachates (g) min.	8.13E-06	7.74E-06	9.28E-06	7.70E-06	7.07E-06	7.54E-06	6.75E-06
Nickel (Ni) in leachates (g) max.	8.18E-06	7.79E-06	9.28E-06	7.79E-06	7.16E-06	7.63E-06	6.79E-06
Antimony (Sb) in leachates (g)	5.04E-08	3.14E-08	3.83E-08	6.98E-08	5.07E-08	5.12E-08	6.61E-08
Barium (Ba) in leachates (g)	2.38E-05	2.07E-05	2.19E-05	1.98E-05	2.05E-05	2.06E-05	1.91E-05
Cadmium (Cd) in leachates (g) min.	3.75E-08	4.98E-08	3.42E-08	4.57E-08	4.03E-08	3.70E-08	4.17E-08
Cadmium (Cd) in leachates (g) max.	5.74E-08	6.34E-08	5.40E-08	6.53E-08	6.02E-08	5.69E-08	6.20E-08
Cerium (Ce) in leachates (g)	6.02E-06	5.22E-06	5.59E-06	5.64E-06	5.73E-06	5.80E-06	5.31E-06
Cesium (Cs) in leachates (g)	3.53E-07	3.12E-07	3.30E-07	3.24E-07	3.18E-07	3.31E-07	2.99E-07
Europium (Eu) in leachates (g)	1.42E-07	1.24E-07	1.29E-07	1.18E-07	1.14E-07	1.19E-07	1.12E-07
Rubidium (Rb) in leachates (g)	4.30E-06	3.84E-06	4.09E-06	3.79E-06	3.65E-06	3.79E-06	3.42E-06
Strontium (Sr) in leachates (g)	3.72E-05	3.30E-05	3.49E-05	3.13E-05	3.12E-05	3.25E-05	2.89E-05
Thorium (Th) in leachates (g)	7.03E-07	5.92E-07	6.59E-07	6.82E-07	7.21E-07	7.41E-07	6.88E-07

Note: See footnotes in Table 4-3.
Note: Presented minimum (min.) and maximum (max.) values incorporate the MDL as described in the text.

Table 4-8 presents measured-to-expected ratios for each impurity calculated by dividing the summed LBL values from Table 4-7 by the expected contribution from the SRM 1632d in each simulated sample (Appendix Table A-2). Results for most elements were reasonably consistent across the seven samples, as indicated by the means and standard deviations (SDs) for the sample set shown in the rightmost column of Table 4-8. Measured-to-expected ratios for 7 of the 18 impurities (Al, V, Mn, Ba, Ce, Rb, and Sr) were well within the estimated uncertainty of the ICP-MS analysis (±10%). Five other impurities (Ca, Fe, Co, Cs, and Th) had a few outlier samples, but means were still within the ±10% measurement uncertainty of the expected values. Measured-to-expected ratios for Cr and Eu were marginally high in most samples. These two elements had above-average blank-to-sample ratios, suggesting nonnegligible background contributions. With blank subtraction applied, Cr and Eu results were in better agreement with the expected contribution from the SRM 1632d in the simulated samples, with mean measured-to-expected

ratios of 1.05 ± 0.05 for Cr and 1.09 ± 0.03 for Eu. Of the remaining four elements, Ti and Sb were clearly undermeasured, and Ni appeared to be overmeasured. However, the Ni content in the SRM 1632d powder was reported by NIST as an information value with an unknown uncertainty, which may affect the conclusion that Ni was overmeasured. Cadmium was unique in that it exhibited the greatest minimum-to-maximum range in the measured-to-expected ratios. This observation was a direct result of Cd having the lowest content of all 18 targeted impurities (see Appendix Table A-2), which was only about six times higher than the MDL. Cadmium was only reliably measured in the first preburn leachates. Inclusion of multiple MDL values in the calculation of the possible maximum summed values for Cd introduced a large additive uncertainty. Considering just the minimum ratios for Cd shown in Table 4-8 (i.e., those based only on measured values), a mean ratio of 1.03 indicated that the measured values were reasonably well-centered around the expected content, but the SD about the mean was higher than for all other impurities. This high sample-to-sample deviation for Cd might be due to a higher ICP-MS measurement uncertainty for concentrations only marginally above the MDL, which has been estimated for these measurements to be ±20%.

Table 4-8. Ratio of measured values in Table 4-7 to expected contributions from SRM 1632d

Impurity in leachate	Leach-Burn-Leach Analysis of Simulated Samples							
	ORNL-A	ORNL-B	ORNL-C	ORNL-D	ORNL-E	ORNL-F	ORNL-G	Mean ± SD
	Combined Leach-Burn-Leach Data (before blank subtraction) / expected contribution from SRM 1632d							
Aluminum (Al)	1.01	0.97	0.95	0.95	0.91	0.95	0.90	0.95 ± 0.04
Calcium (Ca) min.	0.90	0.97	0.88	0.96	0.97	0.97	0.90	0.94 ± 0.04
Calcium (Ca) max.	0.91	0.98	0.89	0.98	0.98	0.98	0.92	0.95 ± 0.04
Titanium (Ti)	0.83	0.72	0.71	0.75	0.72	0.77	0.79	0.76 ± 0.04
Vanadium (V)	0.96	1.00	0.96	0.99	0.96	0.99	0.94	0.97 ± 0.02
Chromium (Cr)	1.05	1.10	1.16	1.13	1.09	1.10	1.10	1.10 ± 0.03
Manganese (Mn) min.	1.00	1.04	1.03	1.04	1.00	1.01	0.98	1.01 ± 0.02
Manganese (Mn) max.	1.00	1.04	1.03	1.05	1.00	1.02	0.99	1.02 ± 0.02
Iron (Fe)	1.26	1.09	0.99	0.97	0.97	1.01	0.99	1.04 ± 0.10
Cobalt (Co)	1.02	1.07	1.03	1.11	1.01	1.05	0.97	1.04 ± 0.04
Nickel (Ni) min.	1.47	1.60	1.76	1.56	1.42	1.54	1.44	1.54 ± 0.12
Nickel (Ni) max.	1.48	1.61	1.76	1.58	1.44	1.56	1.45	1.55 ± 0.11
Antimony (Sb)	0.20	0.15	0.16	0.32	0.23	0.23	0.32	0.23 ± 0.07
Barium (Ba)	1.07	1.05	1.03	1.00	1.02	1.04	1.01	1.03 ± 0.02
Cadmium (Cd) min.	0.85	1.28	0.81	1.16	1.01	0.94	1.12	1.03 ± 0.17
Cadmium (Cd) max.	1.30	1.63	1.28	1.66	1.52	1.45	1.66	1.50 ± 0.16
Cerium (Ce)	0.93	0.92	0.91	0.98	0.99	1.01	0.97	0.96 ± 0.04
Cesium (Cs)	1.07	1.08	1.05	1.10	1.07	1.13	1.07	1.08 ± 0.03
Europium (Eu)	1.19	1.18	1.13	1.10	1.05	1.12	1.10	1.12 ± 0.05
Rubidium (Rb)	1.06	1.08	1.06	1.05	1.00	1.05	0.99	1.04 ± 0.03
Strontium (Sr)	1.06	1.07	1.04	1.00	0.99	1.04	0.97	1.03 ± 0.04
Thorium (Th)	0.89	0.85	0.88	0.97	1.02	1.06	1.03	0.96 ± 0.08

Note: See footnotes in Table 4-7.
Note: Ratios outside the estimated measurement uncertainty of ±10% are highlighted blue (if low) or red (if high).

Further insight into the effectivity of the impurity analysis can be gained by considering the fraction of the total measured amount of each impurity that was dissolved during each leaching stage, as displayed in Figure 4-5 and Figure 4-6 (leachates with less than the MDL were not included in determining the measured fractions shown in these figures). Aluminum exhibited the lowest fraction in the first preburn leach, followed by roughly equivalent fractions detected in the second preburn and first postburn leachates. This result indicates the relatively low solubility of Al prior to the burn phase. After the burn phase, almost all remaining Al was apparently dissolved in the first postburn leach, and the overall analysis for Al was effective, with a mean measured-to-expected ratio of 0.95. Other elements also showed varied degrees of incomplete dissolution prior to the burn, most notably the following: Ti, V, Cr, Ni, Sb, Ba, Ce, Cs, and Rb. With the exception of Ti and Sb, measurements of these elements were

effectively completed by the end of the first postburn leach, with little to no contribution from the second postburn leach.

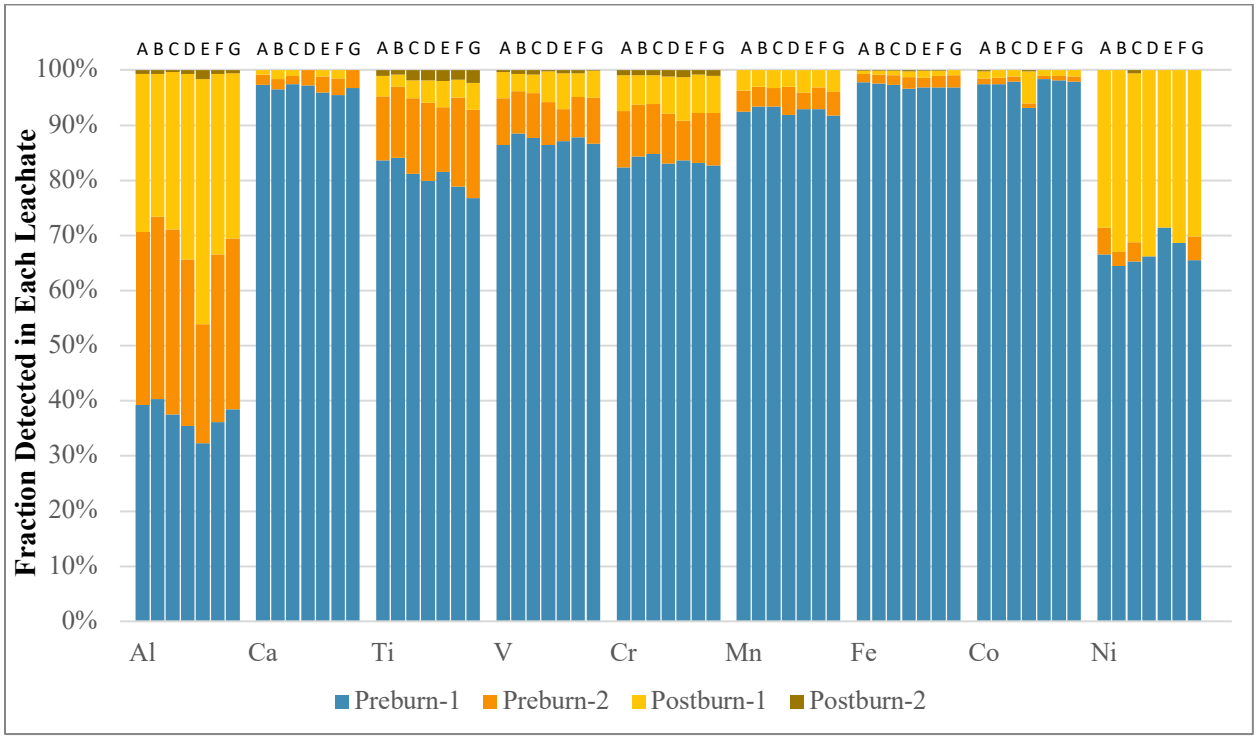

Figure 4-5. Fraction per leach for QC-relevant impurities measured in simulated samples.

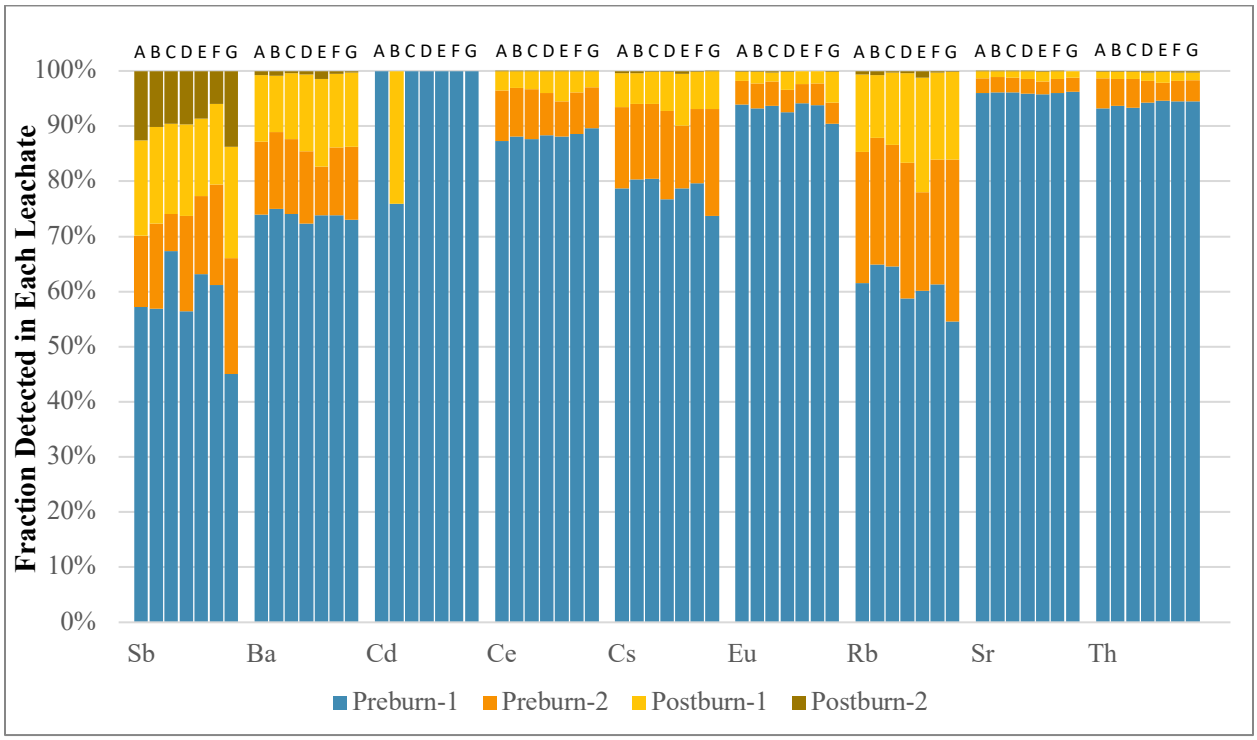

Figure 4-6. Fraction per leach for other targeted impurities measured simulated samples.

The measured-to-expected ratio for Sb (0.15–0.32) was the lowest of all the tracked elements (Table 4-8), and Sb exhibited the largest fractional contribution from the second postburn leach (Figure 4-6). These observations indicate that hot nitric acid leaching was not effective for Sb analysis, which is consistent with observations reported in the literature (Lewińska et al. 2017) because of low solubility of some oxide phases and possible complexing with silica in the boiling vessel walls (Hewitt and Cragin 1991). The summary results in Table 4-8 show that only 0.71–0.83 of the expected amount of Ti in the SRM 1632d was detected with two preburn and two postburn leaches, and Figure 4-6 shows that the relative fraction of Ti detected in the second postburn leaches was low but above average compared with the other elements. These results suggest that undissolved Ti remained after the second postburn leach. Table 4-5 and Table 4-6 show that measurable concentrations of Ti were detected in the third, fourth, and fifth postburn leaches of ORNL-D and ORNL-G, which confirms the presence of some low-solubility Ti after the second postburn leach.

Figure 4-5 and Figure 4-6 show that Ca, Fe, Co, Sr, and Th exhibited nearly complete leaching prior to the burn phase with only minor fractions (1.4% on average) detected after the burn, and Table 4-8 indicates these elements generally exhibited good recovery of the simulated impurities, with the exception of Ca and Th for some samples. The first postburn leach of ORNL-D yielded an abnormally high result for Co, with a measured mass for Co approximately five times higher than the other samples (Table 4-4). Table 4-8 shows that the analysis of ORNL-D also yielded an outlier Co measured-to-expected ratio of 1.11. This higher cumulative result for ORNL-D suggests that its abnormally high first postburn result for Co may not have been related to the SRM 1632d material added to that sample but may possibly have been from Co introduced during the first postburn analysis. The cumulative measured-to-expected ratio for Co in ORNL-D without the first postburn leach data included was 1.04, which is more consistent with the other results for Co presented in Table 4-8.

Preburn solubility was slightly lower for Mn and Eu, in which the fractions detected after the burn phase averaged 3.5% and 2.8%, respectively. However, neglible Mn and Eu were detected in the second postburn leaches, and Table 4-8 indicates these elements also exhibited good recovery of the simulated impurities.

As discussed above, Cd exhibited unusual behavior because the amount introduced by the SRM 1632d powder was barely above the MDL. The only sample that had measurable Cd in a leachate other than from the first preburn leach was ORNL-B, which had less than two times the MDL in the first postburn leachate. As such, the measured result for Cd in the ORNL-B first postburn leachate was highly uncertain. Although the Cd concentration measured in the ORNL-B first postburn leachate was very low, the result contributed to 24% of the total Cd measured in that sample. The measured Cd in the first preburn leachate of ORNL-B represented 97.5% of the expected content from the SRM 1632d powder in the simulated sample, which suggests that the measured amount in the first postburn leachate may not be valid. Excluding the questionable first postburn leach data from ORNL-B yields a mean ± SD for the minimum measured-to-expected ratio of 0.98 ± 0.13 versus the value of 1.03 ± 0.17 reported in Table 4-8.

5. SUMMARY AND CONCLUSIONS

The GIF Very High Temperature Reactor System Fuel and Fuel Cycle Project Management Board coordinated a round-robin test to benchmark and explore the consistency of the methods and results associated with LBL analysis performed on TRISO-coated particle fuel. Results of the ORNL analyses of two sets of LBL round-robin test samples are reported and discussed herein. These results are to be compared with results reported by INET and KAERI in a future summary of the round-robin test. The round-robin test included representative sublots, provided by INET, of TRISO particles with UO_2 kernels fabricated in a production-scale coater. Each round-robin participant received particles riffled from the same parent lot to promote the comparison of different laboratory procedures for the measurement of average uranium loading per particle in addition to the measurement of exposed uranium and a predetermined list of QC-relevant impurities often included in a typical TRISO fuel specification. A second round-robin sample set was produced for each participant by ORNL that contained non-uranium-bearing, TRISO-coated ZrO_2 kernels seeded with a few uranium-bearing TRISO particles with simulated defects, as well as known quantities of a coal powder containing various elements, including the QC-relevant impurities measured in the representative sublots and elements sometimes measured during PIE of irradiated fuel. Particles with simulated exposed-kernel defects or simulated SiC defects were distributed in the simulated samples, as these are the primary coating defects whose presence is detected and enumerated by the LBL procedure (see Section 2.1). These simulated samples were included in the round-robin test to provide insight into the accuracy of the LBL analyses.

The representative sublots received from INET were subjected to uranium-loading analysis and LBL analysis using the general ORNL methodologies described in Sections 2.1 and 2.2. Further details of the specific steps are provided in Section 3, along with results of the analyses for uranium and the requested list of QC-relevant impurities. In addition to LBL analysis of three representative sublots, concurrent analysis was performed on high-purity acid blanks to estimate possible background levels from sources outside the TRISO particles. Measurement results are presented for each leaching stage (two preburn and two postburn) in Section 3.3. Results from each leachate are provided in terms of the mass of each element before and after blank subtraction, and these masses have been converted to ppm to facilitate averaging and direct comparison between results from all the representative sublots measured in the round-robin test, in which some variation in the mass of TRISO particles in each sublot is expected.

Data in this report have been presented with and without blank subtraction to provide insight on how the implementation of blank subtraction can affect results. As discussed in Section 3.3, uranium and other elements measured in the blanks may come from contamination introduced during LBL or ICP-MS. However, the blanks provide only a rough estimate of these background contributions to the values measured in the samples; therefore, background correction via blank subtraction can introduce its own additional uncertainty. When performing LBL for QC acceptance testing, the more conservative approach is to not use the blank-subtracted values for determining if impurities are present above the allowed maximum, thereby avoiding false acceptance of a marginally defective fuel lot. Nevertheless, the blank data can be useful for identifying unusual results that may warrant reanalysis.

No TRISO particles with exposed-kernel defects or SiC defects were detected in the three representative sublots inspected with LBL at ORNL, and the uranium concentrations in the leachates were low but measurably above the background levels suggested by the concurrent LBL analyses of the high-purity acid blanks. Zero particles with exposed-kernel defects or SiC defects out of a total of approximately 90,773 analyzed particles in these three representative sublots yields a 95% confidence interval with an upper bound of ≤3.4E-5 for the defect population in the parent lot. The average amount of uranium measured in the leachates from the three sublots was ~1.4E-7 grams of uranium contamination per gram uranium in the sample.

The measured mass fractions of elemental impurities in the representative sublots were significantly lower than typically specified limits, and in several cases the measured impurity masses were either not significantly higher or even lower than what was measured in the concurrent blank. In these cases, high uncertainty existed regarding how much of the measured element came from the TRISO particles as opposed to external sources introduced during the LBL analysis. In general, the ORNL LBL procedures are not designed to measure the sub-ppm impurity content observed in many of the leachates, as these values would be considered insignificant with respect to the specified limits that the fuel is evaluated against during QC acceptance testing. Reliable measurements of impurity content this low would require more rigorous methods that might include the replacement of glassware for each new analysis and operation in a clean room environment. The predominant impurities measured in the representative sublots were Al, Ca, and Fe, which are not uncommon because these are impurities that have prevalent sources in the laboratory. Measured impurities were generally consistent across the three sublots; however, one sublot (ORNL-DUO2-03T) had measurably elevated content of U, Co, and Ni in the preburn leachates that suggested localized contamination in this sample.

The ORNL results of the LBL analysis of samples with simulated defective particles and added impurities are reported in Section 4. Details of the preparation of the simulated samples are provided in a separate report (Gerczak et al. 2022). That report was updated after completion of LBL by all participating institutions to include information on the number of simulated defects and the mass of various simulated impurities contained in each round-robin sample. A copy of this information for the simulated samples analyzed by ORNL and reported herein can be found in Appendix A. Seven simulated samples were provided to each participating organization. Three samples contained one, two, or four particles with simulated exposed-kernel defects. Three other samples contained one, two, or four particles with simulated SiC defects. A seventh sample contained zero particles with simulated defects. The number and type of defect in each sample is provided in Appendix Table A-1.

Good agreement was found between the LBL analysis results for preburn and postburn leached uranium reported in Section 4.1 and the information in Appendix Table A-1 for number and type of defects in each sample, which demonstrates the effectiveness of the LBL method to detect and enumerate exposed-kernel and SiC defects in TRISO particles. The results for ORNL-A, ORNL-C, and ORNL-F in Table 4-1 indicate that uranium was readily leached from the kernels of particles with simulated exposed-kernel defects during the first preburn leach. The second preburn leachates from these samples contained noticeably elevated but relatively low amounts of uranium compared with the first leaches, which accounted for 99.6–99.7% of the total uranium measured via LBL. The relative fractions detected in the first and second preburn leaches confirm that the two 24 h leaches were sufficient to measure the uranium in the exposed kernels. Similarly, the results for ORNL-E in Table 4-1 indicate that uranium was readily leached from the kernel of one particle with a simulated SiC defect during the first postburn leach of that sample, with 98.9% of the total leached uranium measured in the first postburn leach. ORNL-E had a slightly elevated second preburn leach that indicated some premature leaching prior to the burn. Adding the minor contribution from the preburn leaches to the first postburn leach showed that 99.7% of the total leached uranium was detected by the end of the first preburn leach. However, unlike ORNL-E, sufficient fractions of the uranium in all particles with SiC defects in ORNL-D and ORNL-G were not readily leached by the first postburn leach. The second postburn leachates of ORNL-D and ORNL-G contained 64.7% and 22.3%, respectively, of the uranium measured in the first postburn leachates. Per ORNL LBL procedure, this result required that additional leaching be performed until the measured uranium from successive 24 h leaches dropped off to an acceptably low fraction of the total.

Table 4-1 shows the results from five successive 24 h leaches of ORNL-D and ORNL-G, and Figure 4-2 displays the relative amount of uranium detected in each leach. There was a significant contribution to the total collected during the third postburn leach, after which negligible additional uranium was leached. The total uranium leached from ORNL-G indicated the presence of four particles with SiC defects. However, the total uranium leached from ORNL-D was outside of the combined uncertainties in the individual

kernel uranium content and ICP-MS analysis of the leachates. This result suggested incomplete leaching of at least one particle with a simulated SiC defect persisted. Sorting and analysis of the ORNL-D simulated sample with x-ray imaging techniques revealed that one of the simulated SiC defects contained residual uranium (Figure 4-4), which explained the offset from the expected amount of uranium associated with two particles with SiC defects. The leaching behavior of ORNL-D and ORNL-G appeared to be related to the efficacy of the defect simulation, in which some of the FIB-milled holes used to simulate SiC defects may not have thoroughly penetrated into the IPyC layer or were plugged at some point in the LBL process. The leaching behavior of ORNL-D and ORNL-G illustrates the necessity for including at least two successive leaches in the LBL procedure to provide indication of incomplete leaching and allow the opportunity for additional leaching to increase the confidence in the enumeration of defective particles.

Each LBL round-robin simulated sample contained a known quantity of a coal impurity standard with NIST-evaluated mass fraction values for numerous trace metallic impurities in the powder. The results of the LBL impurity analysis are reported in Section 4.2 and the known quantities in the added impurity standard are listed in Appendix Table A-2. Table 4-8 provides a summary of the results in terms of the ratio of the total measured mass of each impurity element in the LBL leachates versus the expected contribution from the impurity standard. Considering the means and standard deviations for these measured-to-expected ratios over the seven-sample set, the LBL procedure used at ORNL was found to be effective in measuring the impurity content for the majority of elements studied, with a few notable exceptions. Thirteen out of the eighteen elements studied (Al, Ca, V, Mn, Fe, Co, Ba, Cd, Ce, Cs, Rb, Sr, and Th) were measured via LBL to be present in the simulated samples to within ±10% of the expected content in the impurity standard. Two other elements (Cr and Eu) exibited mean measured-to-expected ratios of 1.10 and 1.12, respectively, that could be corrected to less than 10% deviation by applying a background subtraction estimated from the high-purity acid blanks that were processed and measured concurrently with the simulated samples. These deviations were within the estimated uncertainty of the ICP-MS analysis and are considered sufficient for the application of the technique to QC acceptance testing of TRISO fuel impurity content. The Cd content in the coal impurity standard was almost too low to measure, being only six times higher than the MDL. This low content resulted in a much larger scatter in the data because of the elevated uncertainty for such a marginal measurement. Nevertheless, the mean of the measured values from the seven-sample set was still within ±10% of the expected content in the impurity standard.

Only 3 out of the 18 measured impurities were not effectively evaluated. The measured-to-expected ratios for Ni were 1.42–1.76 (Table 4-8). However, the Ni content in the impurty standard was reported by NIST as a low-reliability mass fraction with unknown uncertainty, so no firm conclusion can be drawn from this result. The measured-to-expected ratios were 0.71–0.83 for Ti and 0.15–0.32 for Sb (Table 4-8). Measurable concentrations in the second postburn leachates indicated that these two elements had limited solubility in hot nitric acid, especially in the case of Sb, which showed significant fractional contribution to the measured total in all four leachates plotted in Figure 4-6. These low-solubility issues could be addressed by changing from nitric acid to an acid more suitable for these elements. The use of aqua regia has been determined to be an effective alternative to nitric acid for Sb digestion (Lewińska et al. 2017).

6. REFERENCES

Baldwin, Charles A., John D. Hunn, Robert N. Morris, Fred C. Montgomery, Chinthaka M. Silva, and Paul A. Demkowicz. 2014. "First Elevated Temperature Performance Testing of Coated Particle Fuel Compacts from the AGR-1 Irradiation Experiment." *Nuclear Engineering Design* 271: 131–141.

Demkowicz, Paul A., John D. Hunn, Robert N. Morris, Isabella J. van Rooyen, Tyler J. Gerczak, Jason M. Harp, and Scott A. Ploger. 2015. *AGR-1 Post Irradiation Examination Final Report*. INL/EXT-15-36407, Revision 0. Idaho Falls: Idaho National Laboratory.

Gerczak, Tyler J., Charles A. Baldwin, Grant Helmreich, John D. Hunn, and Fred C. Montgomery. 2022. *Preparation of Simulated LBL Defects for Round-Robin Experiment*. ORNL/TM-2015/722, Revision 3. Oak Ridge: Oak Ridge National Laboratory.

Hewitt, Alan D., and James H. Cragin. 1991. "Comment on 'Acid Digestion for Sediments, Sludges, Soils, and Solid Wastes. A Proposed Alternative to EPA SW 846 Method 3050.'" Environmental Science Technology 25(5): 985–986.

Hunn, John D. 2013. "Leach-Burn-Leach Analysis at ORNL for US VHTR Fuel Development and Qualification." presented at the GIF-VHTR-Fuel and Fuel Cycle Project Management Board Meeting, Cadarache, France, December 12, 2013.

Hunn, John D., Robert N. Morris, Charles A. Baldwin, Fred C. Montgomery, Chinthaka M. Silva, and Tyler J. Gerczak. 2013. *AGR-1 Irradiated Compact 4-4-2 PIE Report: Evaluation of As-Irradiated Fuel Performance with Leach Burn Leach, IMGA, Materialography, and X-ray Tomography*. ORNL/TM-2013/236, Revision 0. Oak Ridge: Oak Ridge National Laboratory.

Hunn, John D., Charles A. Baldwin, Tyler J. Gerczak, Fred C. Montgomery, Robert N. Morris, Chinthaka M. Silva, Paul A. Demkowicz, Jason M. Harp, and Scott A. Ploger. 2016. "Detection and Analysis of Particles with Failed SiC in AGR-1 Fuel Compacts." *Nuclear Engineering Design* 306: 36–46.

Kercher, Andrew K., and John D. Hunn. 2005. *Statistical methods for material characterization and qualification*. ORNL/TM-2005/542, Revision 0. Oak Ridge: Oak Ridge National Laboratory.

Lewińska, Karolina, Anna Karczewska, Marcin Siepak, Bernard Gałka, Michal Stysz, and Cezary Kaźmierowski. 2017. "Recovery and Leachability of Antimony from Mine and Shooting Range Soils." *Journal of Elementology* 22(1): 79–90.

Mackey, Elizabeth A., et al. 2011. *Certificate of Analysis Standard Reference Material 1632d Trace Elements in Coal*. Certificate issue date: October 14, 2014. Gaithersburg: National Institute of Standards and Technology.

Marshall, Douglas W. 2017. *AGR-5/6/7 Fuel Specification*. INL/MIS-11-21423, SPC-1352, Revision 8. Idaho Falls: Idaho National Laboratory.

Morris, Robert N., John D. Hunn, Charles A. Baldwin, Fred C. Montgomery, Tyler J. Gerczak, and Paul A. Demkowicz. 2018. "Initial Results from Safety Testing of US AGR-2 Irradiation Test Fuel." *Nuclear Engineering Design* 329: 124–133.

Petti, David A., John T. Maki, John D. Hunn, Peter J. Pappano, Charles M. Barnes, John J. Saurwein, Scott G. Nagley, James M. Kendall, and Richard R. Hobbins. 2010. "The DOE Advanced Gas Reactor Fuel Development and Qualification Program." *The Journal of The Minerals, Metals & Materials Society* 62(9): 62–66.

APPENDIX A. SIMULATED SAMPLE ANSWER KEY FOR SEEDED DEFECTS AND IMPURITIES

After completion of LBL analysis by all participating institutions, additional information was added to the report, *Preparation of Simulated LBL Defects for Round-Robin Experiment* (Gerczak et al. 2022), to document the number and type of particles with simulated defects that were added to each sample set, as well as the mass of each trace element contained in the added standard reference material—SRM 1632d. Appendix Table A-1 identifies the specific particles with a simulated defect contained in each of the simulated samples analyzed at ORNL with LBL and reported herein (ORNL-A through ORNL-G). Gerczak et al. provided information on these particles in the original report, including images of the defect microstructure of each particle. Appendix Table A-2 (copied from Gerczak et al. 2022) lists the amount of dried SRM 1632d reference material that was added to ORNL-A through ORNL-G and the mass of each impurity in each sample, which was calculated by multiplying the reported mass fraction by the measured mass of added powder. Uncertainty in each calculated impurity mass was propagated from the uncertainties in the mass fraction and measured powder mass. Similar tables were included for the samples sets provided to INET and KAERI.

Appendix Table A-1. Identification of number and type of simulated defects added to each sample

Test sample	Number of simulated defects added	Type of simulated defect added	Particles added
ORNL-A	2	simulated exposed-kernel defect	GIF-41, GIF-42
ORNL-B	0	none	none
ORNL-C	1	simulated exposed-kernel defect	GIF-30
ORNL-D	2	simulated SiC defect	FIB-20, FIB-21
ORNL-E	1	simulated SiC defect	FIB-19
ORNL-F	4	simulated exposed-kernel defect	GIF-43, GIF-44, GIF-49, GIF-04
ORNL-G	4	simulated SiC defect	FIB-23, FIB-25, FIB-26, FIB-27

Appendix Table A-2 includes information from the certificate of analysis for SRM 1632d (Mackey et al. 2011), which is maintained by NIST and can be downloaded from https://www-s.nist.gov/srmors/certificates/archives/1632d.pdf. The certificate of analysis provides detailed information on the standard reference material, including the mass fractions and uncertainties for each element listed in Appendix Table A-2. Certified values are values reported to have the highest confidence for accuracy because all known or suspected biases have been considered. Reference values have uncertainties that may be based only on measurement precision and some sources of uncertainty may not be included. Information values were provided by NIST as they may be of interest and use, but these values were not reported with uncertainties due to insufficient information; therefore, uncertainties for these values are listed in the table as not applicable (NA). Preparation of the simulated samples included acid washing of the ZrO_2-TRISO particles used as a sample base to which the particles with simulated defects and SRM 1632d powder were blended into. As such, the impurities listed in the table should dominate the mass of impurities in each simulated sample, with the exception of uranium for the samples that include simulated defects. The uranium leached from those samples should be dominated by the uranium in the kernels of the particles with simulated defects. The average uranium content in the DUO_2 particles used to make the simulated defects (7.003E-4 g) was ~2600× that of the uranium from the SRM 1632d powder included in each sample.

Appendix Table A-2. Impurity content in SRM 1632d added to each simulated sample

NIST SRM1632d Data			ORNL-A	ORNL-B	ORNL-C	ORNL-D	ORNL-E	ORNL-F	ORNL-G
Mass of dried SRM1632d powder added (g):			0.5529 ± 0.0005	0.4850 ± 0.0005	0.5264 ± 0.0005	0.4922 ± 0.0005	0.4969 ± 0.0005	0.4904 ± 0.0005	0.4672 ± 0.0005
Element	Quality	SRM1632 mass fraction	Mass in sample (g)	Mass in sample (g)	Mass in sample (g)	Mass in sample (g)	Mass in sample (g)	Mass in sample (g)	Mass in sample (g)
Al	reference	9.12E-03 ± 5E-05	5.04E-03 ± 2.8E-05	4.42E-03 ± 2.5E-05	4.80E-03 ± 2.7E-05	4.49E-03 ± 2.5E-05	4.53E-03 ± 2.5E-05	4.47E-03 ± 2.5E-05	4.26E-03 ± 2.4E-05
As	reference	6.1E-06 ± 2E-07	3.37E-06 ± 1.1E-07	2.96E-06 ± 9.7E-08	3.21E-06 ± 1.1E-07	3.00E-06 ± 9.8E-08	3.03E-06 ± 9.9E-08	2.99E-06 ± 9.8E-08	2.85E-06 ± 9.3E-08
B	reference	6.2E-05 ± 1E-06	3.43E-05 ± 5.5E-07	3.01E-05 ± 4.9E-07	3.26E-05 ± 5.3E-07	3.05E-05 ± 4.9E-07	3.08E-05 ± 5.0E-07	3.04E-05 ± 4.9E-07	2.90E-05 ± 4.7E-07
Ba	certified	4.042E-05 ± 8.9E-07	2.23E-05 ± 4.9E-07	1.96E-05 ± 4.3E-07	2.13E-05 ± 4.7E-07	1.99E-05 ± 4.4E-07	2.01E-05 ± 4.4E-07	1.98E-05 ± 4.4E-07	1.89E-05 ± 4.2E-07
C	reference	7.688E-01 ± 1.5E-03	4.25E-01 ± 9.3E-04	3.73E-01 ± 8.2E-04	4.05E-01 ± 8.8E-04	3.78E-01 ± 8.3E-04	3.82E-01 ± 8.4E-04	3.77E-01 ± 8.3E-04	3.59E-01 ± 7.9E-04
Ca	reference	1.44E-03 ± 3E-05	7.96E-04 ± 1.7E-05	6.98E-04 ± 1.5E-05	7.58E-04 ± 1.6E-05	7.09E-04 ± 1.5E-05	7.15E-04 ± 1.5E-05	7.06E-04 ± 1.5E-05	6.73E-04 ± 1.4E-05
Cd	reference	8E-08 ± 1E-08	4.42E-08 ± 5.5E-09	3.88E-08 ± 4.9E-09	4.21E-08 ± 5.3E-09	3.94E-08 ± 4.9E-09	3.97E-08 ± 5.0E-09	3.92E-08 ± 4.9E-09	3.74E-08 ± 4.7E-09
Ce	reference	1.17E-05 ± 4E-07	6.47E-06 ± 2.2E-07	5.67E-06 ± 1.9E-07	6.16E-06 ± 2.1E-07	5.76E-06 ± 2.0E-07	5.81E-06 ± 2.0E-07	5.74E-06 ± 2.0E-07	5.47E-06 ± 1.9E-07
Cl	certified	1.142E-03 ± 1.1E-05	6.31E-04 ± 6.1E-06	5.54E-04 ± 5.4E-06	6.01E-04 ± 5.8E-06	5.62E-04 ± 5.4E-06	5.67E-04 ± 5.5E-06	5.60E-04 ± 5.4E-06	5.34E-04 ± 5.2E-06
Co	certified	3.424E-06 ± 4.8E-08	1.89E-06 ± 2.7E-08	1.66E-06 ± 2.3E-08	1.80E-06 ± 2.5E-08	1.69E-06 ± 2.4E-08	1.70E-06 ± 2.4E-08	1.68E-06 ± 2.4E-08	1.60E-06 ± 2.2E-08
Cr	reference	1.37E-05 ± 1E-07	7.57E-06 ± 5.6E-08	6.64E-06 ± 4.9E-08	7.21E-06 ± 5.3E-08	6.74E-06 ± 5.0E-08	6.81E-06 ± 5.0E-08	6.72E-06 ± 4.9E-08	6.40E-06 ± 4.7E-08
Cs	reference	5.98E-07 ± 6E-09	3.31E-07 ± 3.3E-09	2.90E-07 ± 2.9E-09	3.15E-07 ± 3.2E-09	2.94E-07 ± 3.0E-09	2.97E-07 ± 3.0E-09	2.93E-07 ± 3.0E-09	2.79E-07 ± 2.8E-09
Cu	certified	5.83E-06 ± 3.1E-07	3.22E-06 ± 1.7E-07	2.83E-06 ± 1.5E-07	3.07E-06 ± 1.6E-07	2.87E-06 ± 1.5E-07	2.90E-06 ± 1.5E-07	2.86E-06 ± 1.5E-07	2.72E-06 ± 1.4E-07
Dy	information	9E-07 ± NA	4.98E-07 ± NA	4.37E-07 ± NA	4.74E-07 ± NA	4.43E-07 ± NA	4.47E-07 ± NA	4.41E-07 ± NA	4.20E-07 ± NA
Eu	reference	2.17E-07 ± 6E-09	1.20E-07 ± 3.3E-09	1.05E-07 ± 2.9E-09	1.14E-07 ± 3.2E-09	1.07E-07 ± 3.0E-09	1.08E-07 ± 3.0E-09	1.06E-07 ± 2.9E-09	1.01E-07 ± 2.8E-09
Fe	certified	7.49E-03 ± 1.6E-04	4.14E-03 ± 8.9E-05	3.63E-03 ± 7.8E-05	3.94E-03 ± 8.4E-05	3.69E-03 ± 7.9E-05	3.72E-03 ± 8.0E-05	3.67E-03 ± 7.9E-05	3.50E-03 ± 7.5E-05
H	certified	5.10E-02 ± 5E-04	2.82E-02 ± 2.8E-04	2.47E-02 ± 2.4E-04	2.68E-02 ± 2.6E-04	2.51E-02 ± 2.5E-04	2.53E-02 ± 2.5E-04	2.50E-02 ± 2.5E-04	2.38E-02 ± 2.3E-04
Hf	information	5E-07 ± NA	2.76E-07 ± NA	2.43E-07 ± NA	2.63E-07 ± NA	2.46E-07 ± NA	2.48E-07 ± NA	2.45E-07 ± NA	2.34E-07 ± NA
Hg	certified	9.28E-08 ± 3.3E-09	5.13E-08 ± 1.8E-09	4.50E-08 ± 1.6E-09	4.89E-08 ± 1.7E-09	4.57E-08 ± 1.6E-09	4.61E-08 ± 1.6E-09	4.55E-08 ± 1.6E-09	4.34E-08 ± 1.5E-09
K	certified	1.094E-03 ± 2.6E-05	6.05E-04 ± 1.4E-05	5.31E-04 ± 1.3E-05	5.76E-04 ± 1.4E-05	5.39E-04 ± 1.3E-05	5.44E-04 ± 1.3E-05	5.36E-04 ± 1.3E-05	5.11E-04 ± 1.2E-05
La	information	6E-06 ± NA	3.32E-06 ± NA	2.91E-06 ± NA	3.16E-06 ± NA	2.95E-06 ± NA	2.98E-06 ± NA	2.94E-06 ± NA	2.80E-06 ± NA
Mg	reference	3.90E-04 ± 6E-06	2.16E-04 ± 3.3E-06	1.89E-04 ± 2.9E-06	2.05E-04 ± 3.2E-06	1.92E-04 ± 3.0E-06	1.94E-04 ± 3.0E-06	1.91E-04 ± 2.9E-06	1.82E-04 ± 2.8E-06
Mn	reference	1.31E-05 ± 4E-07	7.24E-06 ± 2.2E-07	6.35E-06 ± 1.9E-07	6.90E-06 ± 2.1E-07	6.45E-06 ± 2.0E-07	6.51E-06 ± 2.0E-07	6.42E-06 ± 2.0E-07	6.12E-06 ± 1.9E-07
N	reference	1.59E-02 ± 1E-04	8.79E-03 ± 5.6E-05	7.71E-03 ± 4.9E-05	8.37E-03 ± 5.3E-05	7.83E-03 ± 5.0E-05	7.90E-03 ± 5.0E-05	7.80E-03 ± 5.0E-05	7.43E-03 ± 4.7E-05
Na	certified	2.969E-04 ± 4.2E-06	1.64E-04 ± 2.3E-06	1.44E-04 ± 2.0E-06	1.56E-04 ± 2.2E-06	1.46E-04 ± 2.1E-06	1.48E-04 ± 2.1E-06	1.46E-04 ± 2.1E-06	1.39E-04 ± 2.0E-06
Ni	information	1.0E-05 ± NA	5.53E-06 ± NA	4.85E-06 ± NA	5.26E-06 ± NA	4.92E-06 ± NA	4.97E-06 ± NA	4.90E-06 ± NA	4.67E-06 ± NA
Pb	certified	3.845E-06 ± 4.2E-08	2.13E-06 ± 2.3E-08	1.86E-06 ± 2.0E-08	2.02E-06 ± 2.2E-08	1.89E-06 ± 2.1E-08	1.91E-06 ± 2.1E-08	1.89E-06 ± 2.1E-08	1.80E-06 ± 2.0E-08
Rb	certified	7.36E-06 ± 2.0E-07	4.07E-06 ± 1.1E-07	3.57E-06 ± 9.7E-08	3.87E-06 ± 1.1E-07	3.62E-06 ± 9.9E-08	3.66E-06 ± 9.9E-08	3.61E-06 ± 9.8E-08	3.44E-06 ± 9.4E-08
S	certified	1.462E-02 ± 7.4E-04	8.08E-03 ± 4.1E-04	7.09E-03 ± 3.6E-04	7.70E-03 ± 3.9E-04	7.20E-03 ± 3.6E-04	7.26E-03 ± 3.7E-04	7.17E-03 ± 3.6E-04	6.83E-03 ± 3.5E-04
Sb	certified	4.45E-07 ± 1.5E-08	2.46E-07 ± 8.3E-09	2.16E-07 ± 7.3E-09	2.34E-07 ± 7.9E-09	2.19E-07 ± 7.4E-09	2.21E-07 ± 7.5E-09	2.18E-07 ± 7.4E-09	2.08E-07 ± 7.0E-09
Sc	reference	2.89E-06 ± 3E-08	1.60E-06 ± 1.7E-08	1.40E-06 ± 1.5E-08	1.52E-06 ± 1.6E-08	1.42E-06 ± 1.5E-08	1.44E-06 ± 1.5E-08	1.42E-06 ± 1.5E-08	1.35E-06 ± 1.4E-08
Se	reference	1.29E-06 ± 3E-08	7.13E-07 ± 1.7E-08	6.26E-07 ± 1.5E-08	6.79E-07 ± 1.6E-08	6.35E-07 ± 1.5E-08	6.41E-07 ± 1.5E-08	6.33E-07 ± 1.5E-08	6.03E-07 ± 1.4E-08
Si	reference	1.65E-02 ± 3E-04	9.12E-03 ± 1.7E-04	8.00E-03 ± 1.5E-04	8.69E-03 ± 1.6E-04	8.12E-03 ± 1.5E-04	8.20E-03 ± 1.5E-04	8.09E-03 ± 1.5E-04	7.71E-03 ± 1.4E-04
Sm	information	1E-06 ± NA	5.53E-07 ± NA	4.85E-07 ± NA	5.26E-07 ± NA	4.92E-07 ± NA	4.97E-07 ± NA	4.90E-07 ± NA	4.67E-07 ± NA
Sr	certified	6.35E-05 ± 1.2E-06	3.51E-05 ± 6.6E-07	3.08E-05 ± 5.8E-07	3.34E-05 ± 6.3E-07	3.13E-05 ± 5.9E-07	3.16E-05 ± 6.0E-07	3.11E-05 ± 5.9E-07	2.97E-05 ± 5.6E-07
Th	certified	1.428E-06 ± 3.5E-08	7.89E-07 ± 1.9E-08	6.93E-07 ± 1.7E-08	7.52E-07 ± 1.8E-08	7.03E-07 ± 1.7E-08	7.10E-07 ± 1.7E-08	7.00E-07 ± 1.7E-08	6.67E-07 ± 1.6E-08
Ti	certified	4.77E-04 ± 1.0E-05	2.64E-04 ± 5.5E-06	2.31E-04 ± 4.9E-06	2.51E-04 ± 5.3E-06	2.35E-04 ± 4.9E-06	2.37E-04 ± 5.0E-06	2.34E-04 ± 4.9E-06	2.23E-04 ± 4.7E-06
U	certified	5.17E-07 ± 1.2E-08	2.86E-07 ± 6.6E-09	2.51E-07 ± 5.8E-09	2.72E-07 ± 6.3E-09	2.54E-07 ± 5.9E-09	2.57E-07 ± 6.0E-09	2.54E-07 ± 5.9E-09	2.42E-07 ± 5.6E-09
V	certified	2.374E-05 ± 1.0E-07	1.31E-05 ± 5.7E-08	1.15E-05 ± 5.0E-08	1.25E-05 ± 5.4E-08	1.17E-05 ± 5.1E-08	1.18E-05 ± 5.1E-08	1.16E-05 ± 5.0E-08	1.11E-05 ± 4.8E-08
Zn	reference	1.29E-05 ± 1.2E-06	7.13E-06 ± 6.6E-07	6.26E-06 ± 5.8E-07	6.79E-06 ± 6.3E-07	6.35E-06 ± 5.9E-07	6.41E-06 ± 6.0E-07	6.33E-06 ± 5.9E-07	6.03E-06 ± 5.6E-07

Note: Listed values for mass fraction ± uncertainty were obtained from NIST SRM 1632d Certificate of Analysis (https://www-s.nist.gov/srmors/certificates/archives/1632d.pdf).
Note: Listed values for mass in sample ± uncertainty were calculated from mass fraction data and measured mass of dry powder added to each simulated sample.
Note: Elements studied in the round-robin test are highlighted yellow for QC-relevant impurities and blue for other tracked elements, including those of interest for PIE.